SPECTRAL ESTIMATION WITH WAVELETS

A Thesis Presented to the

Honors Tutorial College, Ohio University

In Partial Fulfillment of the Requirements for Graduation

from the Honors Tutorial College with the degree of

Bachelor of Science in Physics

David D. McCowan

June 2007

This thesis has been approved by

the Honors Tutorial College and the Department of Physics and Astronomy

---

Dr. David Drabold
Distinguished Professor, Physics and Astronomy
Thesis Advisor

Dr. Thomas Statler
Professor, Physics and Astronomy
Honors Tutorial College Director of Studies, Physics and Astronomy

---

Dr. Ann Fidler
Dean, Honors Tutorial College

Abstract

One of the key problems of data analysis is spectral estimation: the determination of frequencies and amplitudes present in experimental and simulation data. The most popular method is the Fourier transform; however, the Fourier transform has important limitations. Chiefly, it is accurate and reliable only when one frequency is present and when that frequency is stationary (i.e., does not vary with time). Despite these limitations, many continue to use the Fourier transform in suboptimal situations risking nonsensical results. An attempt to overcome these limitations is the continuous wavelet transform, which incorporates temporal information into the analysis, allowing non-stationary (i.e., time-*dependent*) frequencies to be resolved. We have developed and improved techniques for spectral estimation with the wavelet transform using the *Mathematica* computing environment and have applied these techniques to a classic time series to demonstrate our method. In addition, we have applied our technique to new time series from molecular dynamics simulations of carbon trimer molecules and of excited hydrogen atoms in a silicon lattice. Energy decay from the local vibrational modes of the hydrogen into the lattice can be inferred from changes in the amplitudes of the spectral components.

Acknowledgements

It didn't take me long to learn that research is a lot of work. Thankfully, there were quite a few people around to help me through.

First and foremost, I must thank my advisor, Dave Drabold. I still remember bumbling around the department at the end of my sophomore year looking for research opportunities when I first heard Dr. Drabold mention wavelets. At the time, he asked if I had ever heard of them and I timidly replied, "I think so." I have no idea now what I was thinking of at the time, but it certainly wasn't this! Throughout the project, Dr. Drabold was encouraging and engaging. Always willing to drop whatever he was doing to talk, we spent countless hours at his office whiteboard making sketches and (literally) pacing as we both thought aloud. Our discussions ranged from the pressing – molecular vibrations, simulation artifacts, and densities of state – to the colloquial – Wikipedia, coins, and obscure Anglo-Saxon kings (sometimes, all three at once!) Dr. Drabold was optimistic throughout, keeping my spirits high and tempering my moments of anxiety. Along the way, he also served as an invaluable mentor as I dealt with choices for graduate school and life after Ohio University. Without him, completion of this thesis and preservation of my sanity would not have been possible.

Next, I must of course thank those who contributed data to this project. Of main import is Stefan Estreicher of Texas Tech, whose silicon lattice data became our focus for most of the project. Also, I thank Markus Böttcher of Ohio University for contributing blazar light curve data from his own time-frequency investigations and for supplying a fair number of literature leads. Though we never were able to give it a proper analysis, Dr. Böttcher did devote time to discussing blazars and gamma ray bursts with us, and I learned quite a bit along the way.

Next, there are several folks on the wavelet theory end who need to be acknowledged as well. At Ohio University, I had discussions with other wavelet users to get a feel of what research was currently going on. Wow, the diversity! Thanks to Alexander Neiman of Physics and Astronomy; Jeff Connor, Annie Shen and especially Martin Mohlenkamp of Mathematics; and Peter Harrington of Chemistry and Biochemistry.

Of course as one works, one must also eat. I can't forget to thank Honors Tutorial College Dean Ann Fidler and Department of Physics and Astronomy Chair Joe Shields for working out a way to pay me for my first summer of work.

Finally, there are those who helped in the editing stage. Having dealt with wavelets for over a year, I know that continuous transforms don't use orthogonal wavelets. Sometimes I need others to point out that it's not common knowledge. Thanks to Daniel Hoy, Colin McCrone, and Michael Newman for their help on this front.

June 1, 2007
Athens, Ohio

Introduction

Determining frequencies present in data has long been of significant interest to scientists. Different techniques for such determination, known as spectral estimation, have come from many varying branches including mathematics, engineering, economics, physics, biology, geology, meteorology, and, in short, any field that deals with data that change over time.

This thesis explores a relatively new technique for spectral estimation called the continuous wavelet transform. Our work details the development and implementation of wavelet techniques and our application of the wavelet transform to various data sets in physics.

Chapter 1 is a review of several spectral estimation techniques and describes how these techniques fail to properly detect non-stationary frequencies and amplitudes. This review sets the stage for the introduction of the wavelet transform at the end of the chapter. A full discussion of the wavelet transform – mathematical foundations, different wavelets, and interpretation – follows in Chapter 2.

Chapter 3 marks the beginning of our original research with the wavelet transform. This chapter covers our choice of wavelet and the development and

refinement of techniques for using it. Chapter 4 details the application of the wavelet transform to a various data series. It opens with a demonstration of the power and accuracy of the technique based on results from analysis of a classic time series and is followed by the application of the transform to new data, most notably our study of energy transfer in a system of excited hydrogen atoms imbedded in a silicon lattice.

Chapter 5 contains conclusions, thoughts on improvements and possible avenues for new research.

This thesis is a useful demonstration of the wavelet transform's ubiquity in spectral estimation and goes so far as to show its ultimate necessity in certain situations. Many fields, physics among them, have lagged behind in adopting this rather important technique and it's time for change; the adage that old habits die hard appears to be true[1]. This thesis is a suitable beginner's guide to the transform as well as a demonstration of its applicability to physics data analysis, but in many ways it is a push. It is a push to the scientific community to get up and get smart about what the options are. The wavelet transform is here to stay.

[1] As another example, I note that a healthy portion of the physics community still uses the computer programming language FORTRAN, which was invented in the 1950s when computers took up entire buildings. Though most physicists will defend it on a number of points, I once brought this up in the company of a computer science major who irreverently laughed at me.

Chapter 1 Spectral Estimation

Spectral estimation is one of the most common forms of data analysis. This first chapter details the basics of spectral estimation and identifies a number of common techniques. What is presented here is hardly exhaustive, but will suffice to show that non-stationary data deserve careful treatment and most current techniques cannot properly deal with them. The most general and best technique for such situations is the wavelet transform.

1.1 Time Series and Functions

A time series is any set of data points that describes a quantity at different points in time. It is usually given as a string of N numbers, $\{f_n\} = f_0, f_1, f_2, \ldots, f_{N-1}$, where the points are sampled at equal time intervals. It may also be given as ordered pairs of time and value, $\{(t_n, f_n)\} = (t_0, f_0), (t_1, f_1), (t_2, f_2)\ldots, (t_{N-1}, f_{N-1})$, where the points may or may not be sampled at equal time intervals. Most experiments or computer simulations yield data in the form of a time series. For a physicist, an example of a time series might be the instantaneous velocities of a particle as it moves along a trajectory; for an economist, the price of a stock on each day of a given year; and for a

biologist, the number of salmon in a river over a given time period. For simplification, most equations and discussions in this thesis will refer not to discrete time series, but to functions of time, *f(t)*. Time series can be thought of as samples of a function; $\{f_n\}$ = $f(t_0), f(t_1), f(t_2), \ldots, f(t_{N-1})$, so there is no loss of generality.

Analysis of time series (or functions) can provide information not readily available from the raw data points. Principally, investigations are done to learn about the characteristics of the series (e.g., frequency or noise content, chaotic behavior, trends) or to make predictions about the future of the series. In this thesis, our main concern is the frequency content; that is, spectral estimation. We are interested in which frequencies are present and how their amplitudes change over time.

A time series that is being analyzed is often called a signal. Oscillatory signals can be expressed as the sum of functions of the form $f(t) = A(t)\cos[\varphi(t)]$ where $A(t)$ is the amplitude of the signal and $\omega = \partial\phi / \partial t$ is its frequency.[2,3] A signal is considered to be stationary if the amplitudes and frequencies present do not vary with time. An example of a stationary signal is the function $f(t) = \sin(t)$ which has frequency $\omega = 1$ and amplitude $A = 1$ for all time, *t*. A signal is non-stationary if the amplitudes or frequencies are time-dependent. Examples of non-stationary signals include $f(t)=\sin(t^2)$ with $\omega = \frac{1}{2}t^2$ and $A = 1$, and $f(t) = e^{-t}\sin(2t)$ with $\omega = 2$ and $A = e^{-t}$.

[2] The choices of $A(t)$ and $\varphi(t)$ are not unique. It is convenient to define a canonical representation given by the analytic signal defined as $Z(t) = A(t)\exp[i\varphi(t)] = [\,1 + i\mathcal{H}]\, f(t)$ where $\mathcal{H}$ is the Hilbert transform. A full discussion of this representation can be found in [1].

[3] Properly, ω is the angular frequency and is related to "normal" frequency (*f* or *ν*) by $\nu = \omega / 2\pi$. I will often refer to both as frequency in general and have clarified in cases where ambiguity may arise.

It should also be pointed out that the time series is only one specific type of data series. All the results mentioned here and below are applicable to space series, as well, simply by replacing the time variable *t* with coordinate variable *x*, *y*, *z*, *r*, etc. as needed. In such instances, frequency would refer to spatial frequency instead of temporal frequency and so on. Examples of space series include density measured at given distances from a point and atmospheric pressure at different altitudes.

1.2 The Fourier Transform

The Fourier transform is perhaps the most common method for extracting the spectral content of a signal. Applying this transform decomposes a signal from the time domain (with no explicit frequency information) into the frequency domain (with no time information). The transform is given by the formula

$$\hat{F}(\omega) = \int_{-\infty}^{\infty} f(t) e^{-i\omega t} dt .$$

Because the result of the Fourier transform is a complex function, $\hat{F}(\omega) = \Re + i\Im$, it can be expressed in terms of its modulus and phase, given (respectively) by

$$A(\omega) = \left|\hat{F}(\omega)\right| = \sqrt{\hat{F}(\omega)\hat{F}^{*}(\omega)} \text{ and}$$

$$\phi(\omega) = \tan^{-1}\left(\frac{\Im(\omega)}{\Re(\omega)}\right)$$

such that $\hat{F}(\omega) = A(\omega)e^{i\varphi(\omega)}$. For spectral estimation, the results are displayed as plots of the modulus squared (also referred to as the Schuster periodogram [2] or power

spectrum). Large peaks in the Fourier plot appear at frequency values that are present in the function or series. The plot shows values close to or equal to zero at frequencies that are not present in the signal (Figure 1-1). The phase is used if a reconstruction of the original series or function is needed.

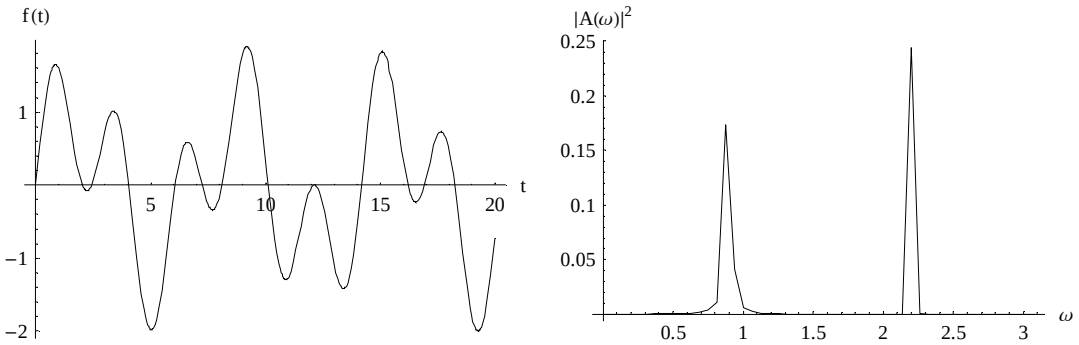

Figure 1-1: The signal $f(t) = \sin(0.9t) + \sin(2.2t)$ is plotted on the left. Its Fourier transform is shown on the right[4]. Note that the two frequencies $\omega = 0.9$ and $\omega = 2.2$ are clearly present as spikes in the periodogram.

The Fourier periodogram, however, can be misleading. First, no time information is preserved from the original function or series; therefore, it is impossible to accurately detect non-stationary frequencies. For example, if a single frequency is present in a signal but it varies over time, the peak in the periodogram may broaden giving the illusion of a continuum of frequencies (Figure 1-2). If multiple frequencies are present in a signal, but appear at different, non-overlapping times (i.e., are piecewise constant), all frequencies will appear in the periodogram but there will be no evidence of their time separation (Figure 1-3). Second, the Fourier transform gives optimal results only when a single frequency is present. If the signal contains multiple

[4] Throughout this paper, a discrete Fourier transform is used. Hence, peaks in the periodogram are not true delta functions, but have finite width.

frequencies, the transform may have difficulties resolving close frequencies, assigning accurate relative amplitudes or separating out noise. A more detailed description and derivation of these limitations can be found in [3].

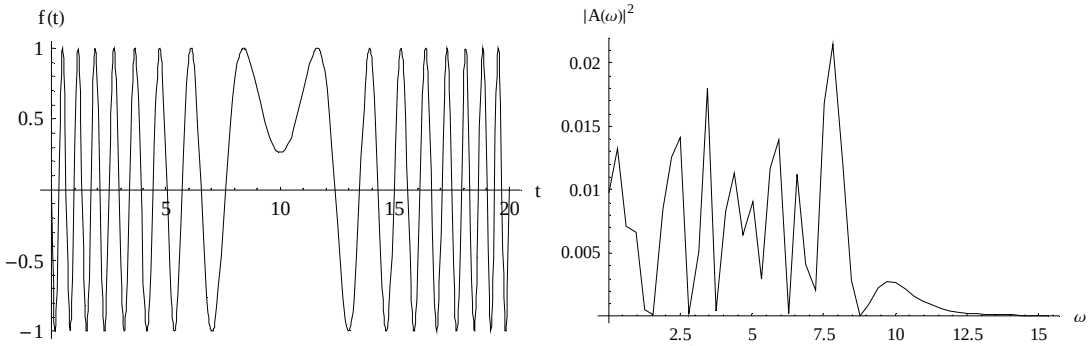

Figure 1-2: The non-stationary signal *f(t)*=sin(*0.5t²-10t)* is plotted on the left. Its Fourier transform is plotted on the right. The Fourier plot gives the (false) impression that several closely spaced discrete frequencies are present in the signal.

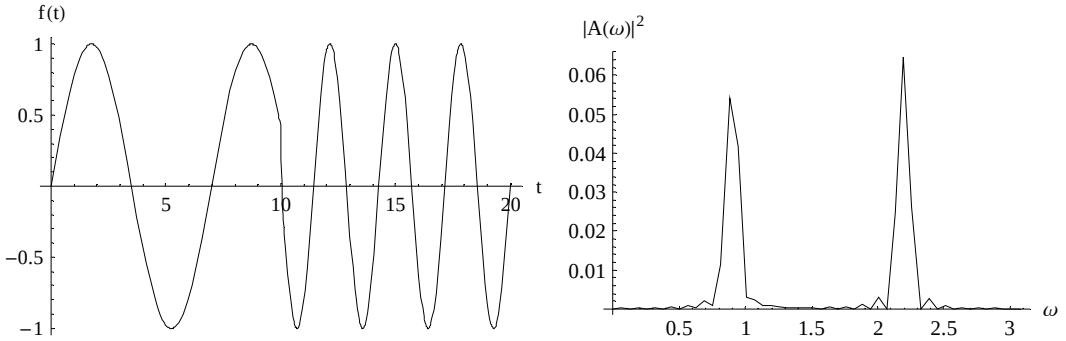

Figure 1-3: The signal $f(t)=\begin{cases}\sin(0.9t), & 0\le t\le 10\\ \sin(2.2t), & t>10\end{cases}$ is plotted on the left. Its Fourier transform is shown of the right. A comparison to Figure 1-1 shows that the two periodograms are nearly identical and differ only in amplitude. (Because these frequencies were present for half the time period as those in Figure 1-1, their amplitude is $\left(\frac{1}{2}\right)^2=\frac{1}{4}$ of the previous value.) The non-stationarity of the series is completely hidden.

1.3 Time-Frequency Analysis

If a signal is non-stationary, conventional frequency analysis techniques are ineffective. Techniques that incorporate both time and frequency into the result must be used. The goal of time-frequency analysis is not only to estimate the spectral content of a signal, but to find how the frequencies and their amplitudes change over time. Several methods of time-frequency analysis are now addressed.

1.3.1 Bayesian Spectral Analysis[5]

Another approach to estimating frequencies is to use probability techniques. If *A* and *B* are propositions and we let $P(A|B)$ represent the probability that A is true given that B is true, then Bayes' theorem is states that

$$P(H \mid D, I) = \frac{P(H \mid I)\, P(D \mid H, I)}{P(D \mid I)}$$

where *H* is the hypothesis (i.e., the model being tested), *D* is the data (i.e., the time series to be analyzed), and *I* is any prior information (i.e., any known constraints on the model). In spectral analysis, the model representing the estimated true signal, "f(t)", is expressed in its most general form as

$$H = \text{" } f(t) \text{"} = \sum_{j=1}^{N} B_j G_j(t, \{\omega\})$$

where G_j is a function such as a sinusoid or sum of sinusoids, $\{\omega\}$ is a set of frequencies being tested and B_j is the amplitude of the function. Therefore, for spectral

[5] Complete treatments of Bayesian spectral analysis can be found in [3] and [4].

estimation, Bayes' Theorem expresses the probability that the model describes the data in the form

$$P(\omega, B \mid D, I) = \frac{P(\omega, B \mid I)\, P(D \mid \omega, B, I)}{P(D \mid I)}.$$

where $P(\omega, B \mid I)$ is called the posterior probability density, $P(\omega, B \mid I)$ is the prior, $P(D \mid \omega, B, I)$ is the likelihood, and $P(D \mid I)$ is a normalization constant. This form thus estimates the probability that frequency ω is present with amplitude B in the data (D) given any prior constraints (I).

In the case of stationary signals with a single frequency present, the model takes the simple form of

$$"f(t)" = B_1 \sin(\omega t) + B_2 \cos(\omega t),$$

and the posterior probability density has three parameters (B_1, B_2, ω) which it estimates. A more complex model can be assumed to account for additional frequencies, time-dependent frequencies or amplitudes, or noise. The posterior probability can also be modified to eliminate parameters that are not of interest by integrating over these parameters. For example, assuming two parameters, B and ω, the posterior probability density that a given frequency is present is

$$P(\omega \mid D, I) = \int P(\omega, B \mid D, I)\, dB.$$

Bayesian spectral estimation has the advantage that it allows the user to incorporate prior knowledge about the signal into the calculation through model selection and the constraint, I. It also has the advantage of being able to handle non-stationary data. However, if no prior information is known about a signal, model

selection degenerates into conventional least squares fitting of the likelihood function. The Bayesian approach offers a rigorous framework for analyzing the spectral content, particularly in the presence of noise.

1.3.2 Windowed Fourier (Gabor) Transform

Another technique for time-frequency analysis is the windowed Fourier transform (also known as the short-time Fourier transform or the Gabor transform [5]). Here, the signal is Fourier transformed not as a whole function or series, but in small pieces, called windows, along the length of the signal. Therefore, frequency information is localized for each window and is independent of the behavior of the signal at other times. This windowing is accomplished by the time-frequency atom,

$$w(t)e^{-i\omega t},$$

where $\omega(t)$ is a window function which is zero outside a short, finite interval and $\exp(i\omega t)$ is the Fourier transform oscillation term. Examples of window functions are included in Figure 1-4. The formula for the windowed Fourier transfom is

$$\breve{F}(\omega,\tau) = \int_{-\infty}^{\infty} f(t)w(t-\tau)e^{-i\omega t}dt,$$

where the window function (and thus the frequency information) is centered at time τ. Plots are called spectrograms and usually show time and frequency vs. modulus squared in 3D or contour. Local maxima in the plot reveal what frequencies are present at what times.

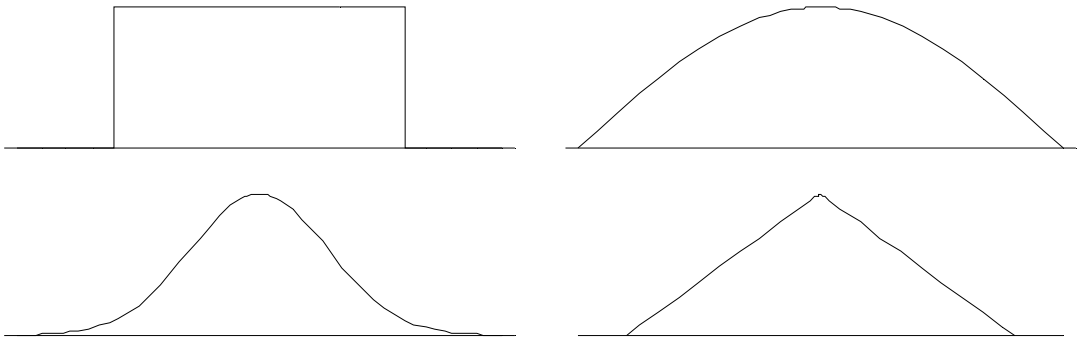

Figure 1-4: Examples of common window functions. Clockwise from top left: box, truncated sinusoid, Gaussian, triangle.

While the windowed Fourier transform makes strides toward better detection of non-stationarity, it still falls short due to the problem of fixed resolution. Once a window is chosen, the time and frequency resolutions (the ability to distinguish between close times and frequencies respectively) are set (Figure 1-5)[6]. Choosing a window which is too narrow will cause the transform to fail to separate or detect low frequencies whose wavelengths are larger than the size of the window. However, choosing a wider window worsens the temporal resolution because larger intervals of signal are analyzed at once (see Figure 1-6). Unless some information is known *a priori* about the nature of the expected frequencies, choosing a window size must be done through trial and error and even with such knowledge, a suitable compromise between temporal and spectral resolutions may not be possible.

The problem of fixed resolution is remedied by introducing multiresolution analysis, of which the most common method is the wavelet transform.

[6] Time resolution can be defined as the standard deviation of the modulus squared atom, $|w(t) \exp[i\omega t]|^2$. Frequency resolution is the standard deviation of the modulus squared of the Fourier transform of the atom. Both are set only by the width of the window and are constant for all frequencies [7].

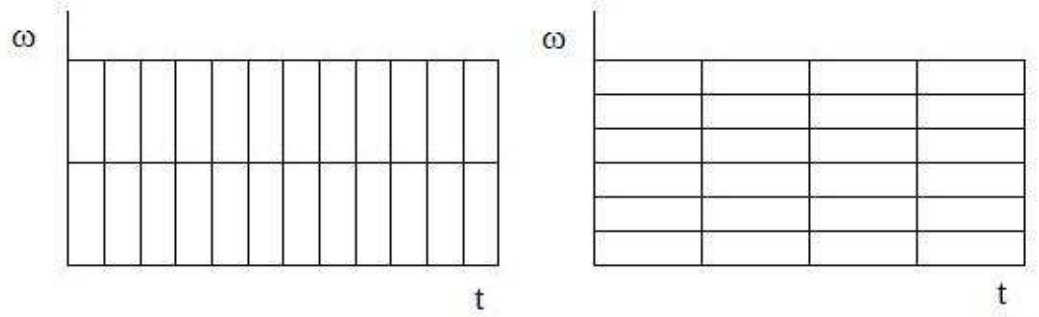

Figure 1-5: The length and width of the blocks represent the time and frequency resolutions for a particular window. The plot on the left represents a window with good time resolution but poor frequency resolution. The plot on the right represents a window with good frequency resolution but poor time resolution.

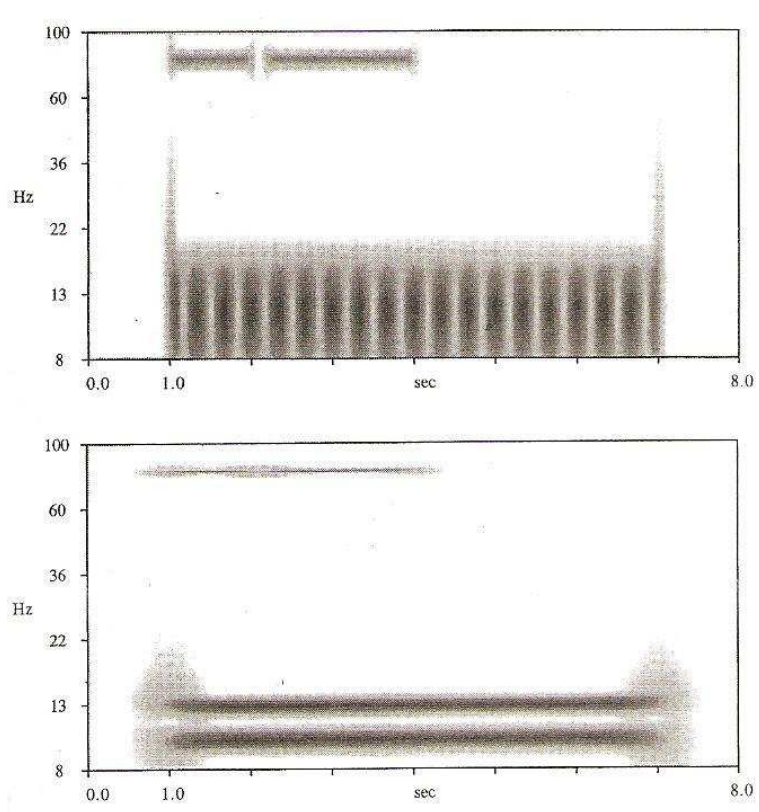

Figure 1-6: Both graphs display the contour plot of the windowed Fourier transform spectrograms of a sound signal. The signal contains constant frequencies at v=10Hz and v=13Hz sustained from t=1s to t=7s as well as a frequency at v=80Hz present from t=1s to t=5s with a gap at t=2s. In the top plot, a window which was too narrow was used; time resolution is excellent (note the gap in the v=80Hz frequency), however the two low frequencies could not be separated. In the bottom plot, a window which was too wide was used; the low frequencies are resolved, but the gap in the high frequency is gone. (Source: [6].)

1.3.3 Wavelet Transform

The aim of the wavelet transform is the same as the windowed Fourier transform: to estimate spectral content of a signal and describe its change over time. To do this, the wavelet transform combines the Fourier oscillating term and the window term, *w(t)*, into one function, the wavelet, $\Psi(t)$. Examples are given in Figure 1-7. The formula for the wavelet transform is

$$\tilde{F}(a,b) = \frac{1}{a}\int_{-\infty}^{\infty} f(t)\,\Psi^{*}\left(\frac{t-b}{a}\right)dt\,,$$

where the star denotes the complex conjugate of the wavelet. This result is a function of two variables: *a*, the scale, and *b*, the translation. The scale shrinks or expands the width of the wavelet while keeping the number of oscillations constant. The translation moves the wavelet along the time axis of the signal.

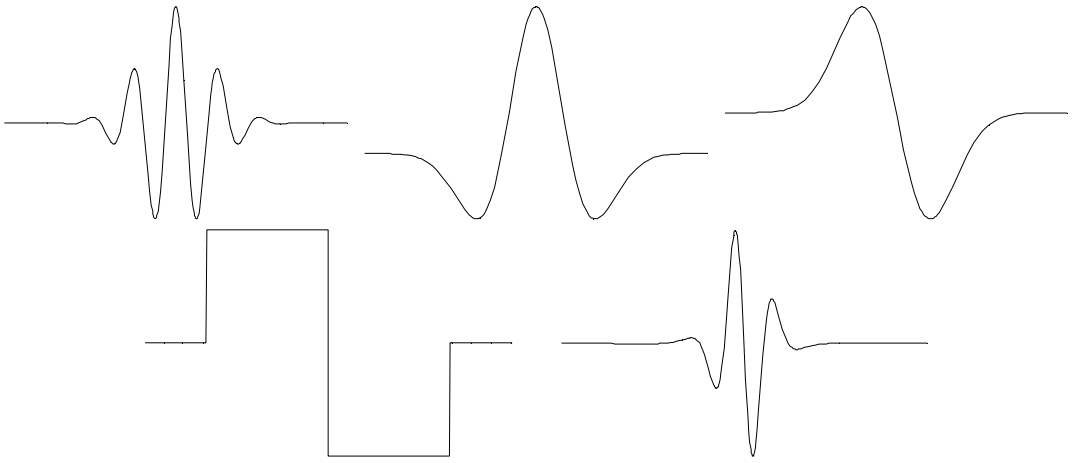

Figure 1-7: Examples of wavelets.

The power of the wavelet is in the concept of scale. As *a* is changed, a range of frequency values is swept while simultaneously adjusting the window size. The

transform provides better frequency resolution at low frequencies and better time resolution at high frequencies (Figure 1-8)[7]. In nature, high frequencies generally tend to be transient and short-lived while low frequencies generally tend to persist, so this resolution adjustment is ideal. (Figure 1-9).

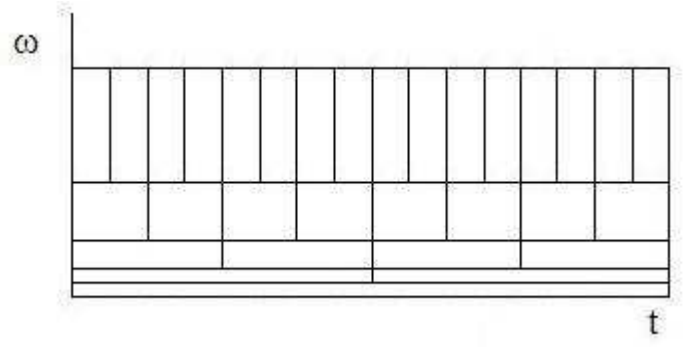

Figure 1-8: As in Figure 1-5, the length and width of the blocks represent the time and frequency resolutions for a particular window. Wavelets have the desirable property that these resolutions change at different scale values.

The plot of the wavelet transform is called a scalogram and graphs scale and time versus modulus. Scale can be changed to frequency through a conversion unique to the choice of wavelet, and the resulting plot is then called a time-frequency representation. As with the windowed Fourier transform, local maxima, called ridges, give the frequency content as a function of time.

[7] Similarly to the windowed Fourier transform case, the time resolution is the standard deviation of the modulus squared wavelet and the frequency resolution is the standard deviation of the modulus squared Fourier transform of the wavelet. Note here, however, that these values are not fixed, but vary with scale because the size of the effective window changes [7].

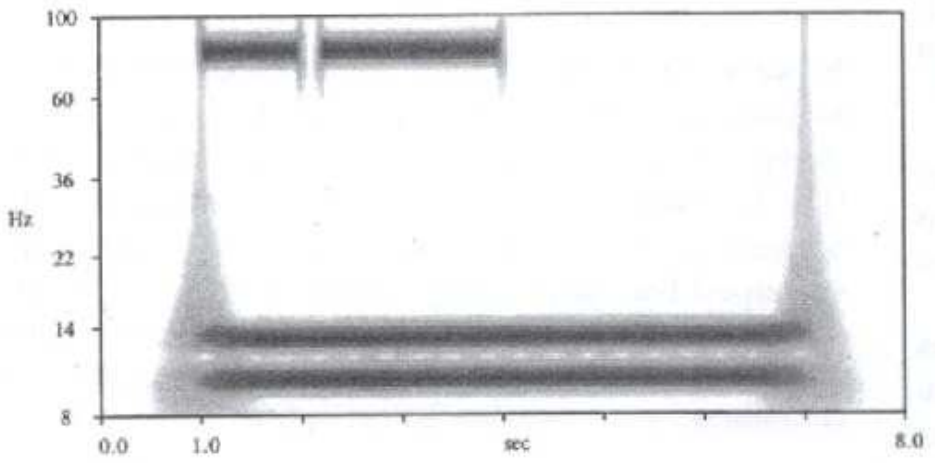

Figure 1-9: The contour plot of the wavelet transform of the signal in Figure 1-6. Note that both the low frequencies are resolved as is the time gap in high frequency signal (Source [6].)

Chapter 2 The Wavelet Transform

Now that the wavelet transform has been introduced as an improved tool for non-stationary spectral estimation, it is necessary to delve a little deeper into the details. The first half of this chapter covers the basics, dealing with what a wavelet is and what the transform reveals. The second half of the chapter is more mathematically intense, covering topics such as wavelet choice and the conversion from wavelet scalogram to full time-frequency representation.

2.1 Wavelet and Transform Basics

2.1.1 History[8]

The oldest and most common method of spectral estimation is the Fourier transform. While it is the oldest method, its popularity is more likely due to wide availability and computational quickness of the fast Fourier transform algorithm (FFT) which cuts the number of computations needed for n data points from n^2 to $n \ln(n)$. With the invention of computers, it became possible to efficiently calculate Fourier

[8] A more complete history of the development of the wavelet transform, told in a non-technical, easy to follow way, can be found in [8].

transforms of long series that had never been examined before. Thus, a headlong push to use the FFT for anything and everything began which has, many may argue, never stopped [8]. However, the Fourier transform, as has already been explained, is not always the best choice. Two excellent quotes capture the absurdity of the FFT or bust mentality. First, Yves Meyer:

> Because the FFT is very effective, people have used it in problems where it is not useful – the way Americans use cars to go half a block. Cars are useful, but that's a misuse of the car. So the FFT has been misused, because it's so practical (as quoted in [8]).

And, Barbara Burke Hubbard:

> In some cases, scientists using [the FFT] are like the man looking for a coin under a lamppost, not because that is where he dropped it, but because that's where the light is [8].

For those aware and conscious of the limitations of the Fourier transform though, the only suitable option for non-stationary analysis was, for a long time, the windowed Fourier transform with its own inadequacies.

Several attempts toward improving the windowed Fourier transform can be found from the 1960s and 1970s, but what is usually quoted as the beginning of the modern wavelet transform was the 1984 development by geophysicist Jean Morlet and quantum theorist Alex Grossman of the "cycle octave transform" [9]. Motivated by non-stationary time series encountered in the detection of buried oil deposits, they built up wavelet theory and stumbled upon many remarkable features such as time-frequency localization and perfect signal reconstruction. The concept lingered and developed slowly [10], and the name *cycle octave transform* was abandoned for the less awkward *wavelet transform,* named for their "wavelets of constant shape" [8].

The wavelet transform really took off though, after attracting the attention of mathematical physicist Ingrid Daubechies. Her 1988 and 1990 papers and 1992 book gave wavelets a rigorous mathematical foundation and propelled them into practical use [11], [12], [13].

Today, the wavelet transform finds use in a number of fields, principally economics, finance, meteorology, climatology, computing, engineering and mathematics. Their use is growing in the sciences, but wavelet techniques have yet to overtake Fourier analysis *en masse*, even in instances of non-stationarity. By 2001 however, over 1000 peer-reviewed journal articles were being published on wavelets per year [7].

2.1.2 Wavelet Basics

A wavelet can be thought of as a localized wave. Whereas a wave has a defined shape that extends to infinity without attenuation, a wavelet only oscillates over a small region and then tends to zero outside that interval (Figure 2-1).

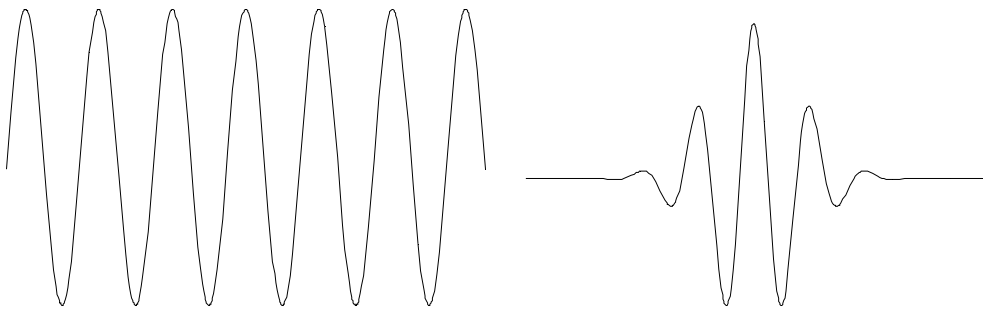

Figure 2-1: A wave (infinite) on the left and a wavelet (localized) on the right.

Think back to the Fourier transform. It compares the signal to different waves, but in each case, the wave has constant frequency over the entire signal. In the windowed Fourier case, the analyzing wave is truncated and localized by a window, but the window size remains the same for each frequency. Thus, as higher frequencies are reached, more and more oscillations are fit into the window (Figure 2-2, *top*).

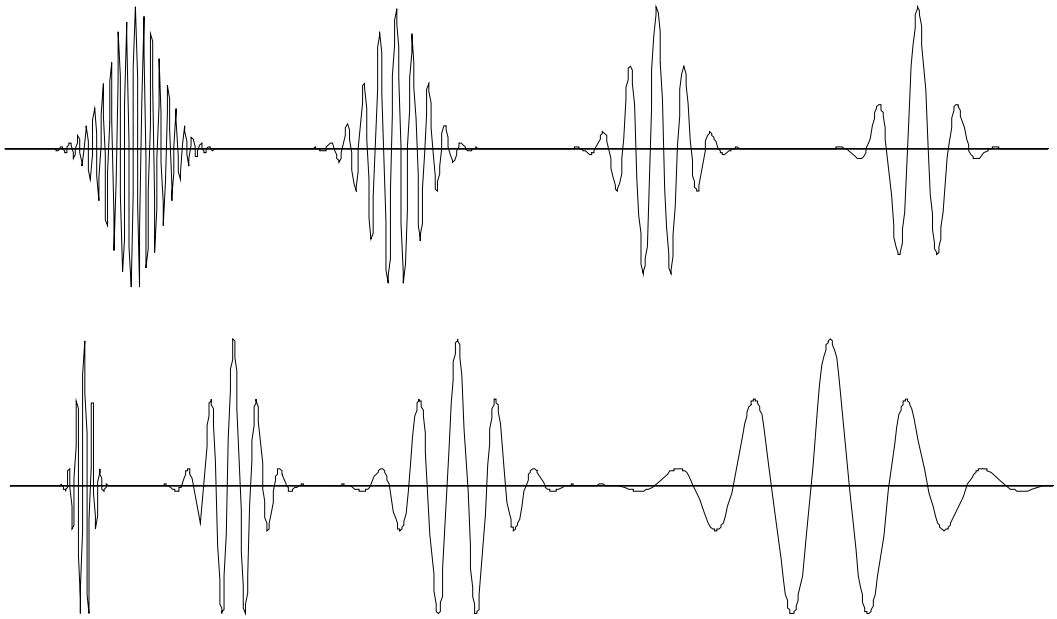

Figure 2-2: In the top plot, windowed Fourier transform time-frequency atoms are shown with progressively decreasing frequencies. Note that the window size stays constant while the number of oscillations contained within decreases. In the bottom plot, a wavelet is scaled to higher values of *a* (i.e., lower frequency). Note that the size of the effective window changes while the number of oscillations does not.

The wavelet transform is different. By using wavelets that are scaled (squeezed or expanded), the number of oscillations within the effective "window" remains constant; it is the *shape* of the wavelet that changes (Figure 2-2, *bottom*). This subtle difference gives the wavelet transform considerably more power than the windowed

Fourier transform. As addressed in Chapter 1, the time and frequency resolutions change as the wavelet is scaled, giving better time resolution for small windows and better frequency resolution for large ones.

2.1.3 Transform Basics

The wavelet transform is defined mathematically as a convolution of the signal and the wavelet. While such a statement is rigorous and has precise mathematical meaning, it does not help much in understanding what is happening and why the transform works at all.

In a convolution, two functions (here the signal and the wavelet) are multiplied together and integrated. When the signal and the wavelet both have similar features and align well in time, their product is large and the area beneath this curve is also large. If the two have similar shapes, but do not align well in time (i.e., are out of phase), the product and area are both large, but negative. When the signal and the wavelet are dissimilar, the area beneath their product will tend toward zero because, on average, the product (and therefore area) will be positive as often as it is negative. This is illustrated in Figure 2-3.

When real-valued wavelets are used, the resulting scalogram gives closely spaced maxima and minima where the wavelet and signal correspond well with each other (Figure 2-4, *top*). Thus, large transform amplitudes reveal that a given scale (frequency) is present in the signal while amplitudes close to zero represent a lack of that scale (frequency) in the signal.

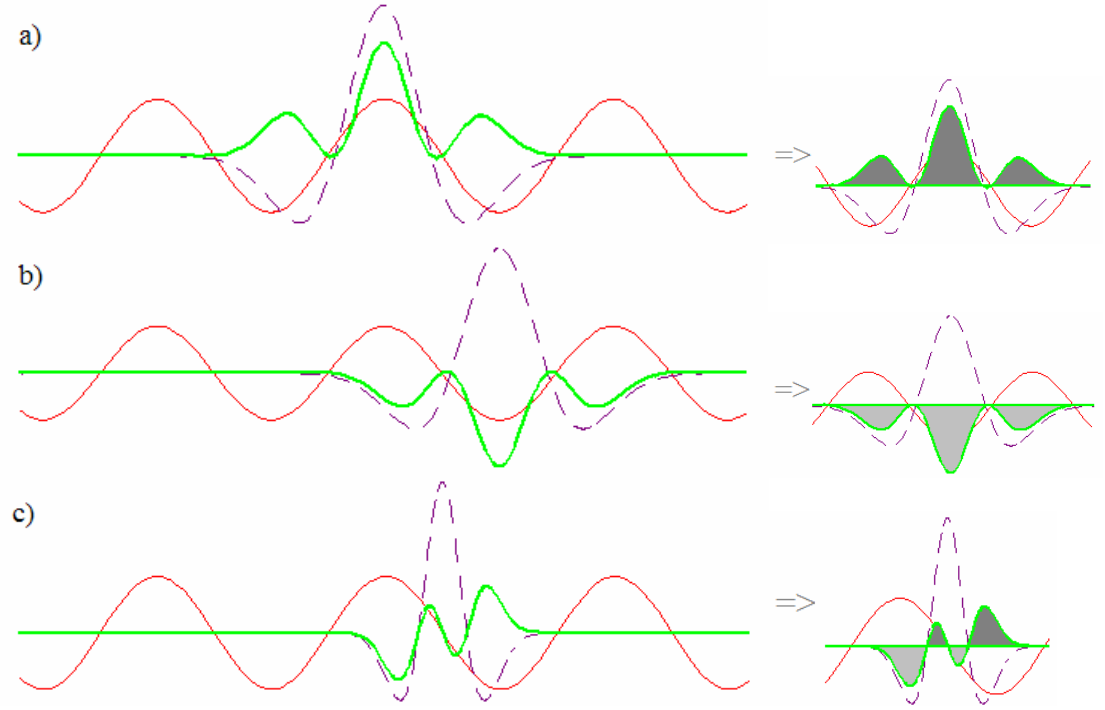

Figure 2-3: In this schematic of the wavelet transform convolution, the signal is plotted in solid red, the wavelet is plotted in dashed purple and their product is plotted in thick green. The area beneath the product is displayed to the right with dark grey representing positive contribution to the transform and light grey representing negative contribution.

(a) The wavelet and signal have similar shape and align well in time. The contributions are all positive and therefore the transform result is positive.
(b) The wavelet and signal have similar in shape, but out of phase. The contributions are all negative and therefore the transform result is negative.
(c) The wavelet and signal are dissimilar and have no time correlation. The contributions are equally positive and negative, so the result is zero.

For complex-valued wavelets, the situation is similar. If the signal and the real part of the wavelet match well in shape and time, a large real transform amplitude is produced. If the signal and the imaginary part likewise match, a large imaginary transform amplitude is produced. Note though, that because the real and imaginary parts of the wavelet are out of phase to each other, maxima (or minima) in the real and imaginary transform amplitudes are equally out of phase. Therefore, when the

modulus of the transform is taken, both parts contribute and the closely spaced maxima and minima seen in the real-valued wavelet case are replaced by smooth, continuous ridges (Figure 2-4, *bottom*). This incorporation of phase is important, especially if information about how the ridge amplitude changes over time is desired. As many non-stationary signals have time-dependent amplitudes, complex-valued wavelets are preferred for spectral estimation.

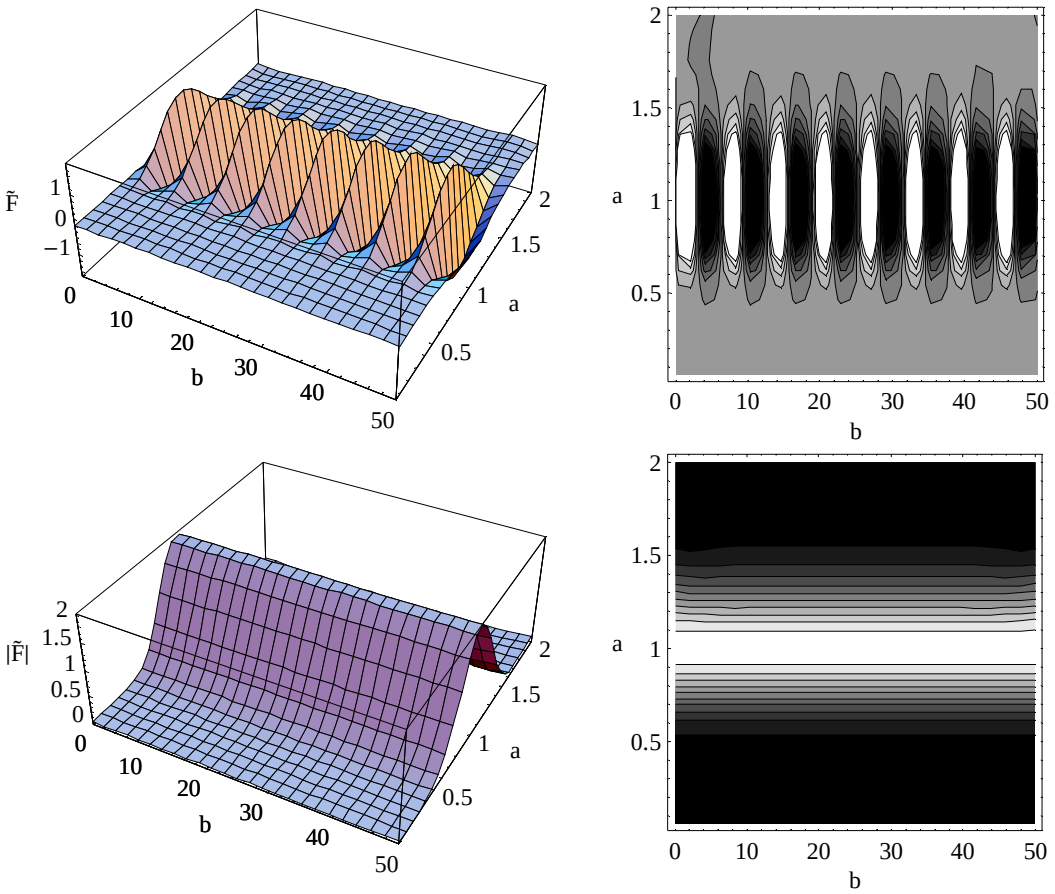

Figure 2-4: Wavelet transforms of the signal *f(t)*=sin*(t)* are plotted in 3D (left) and contour (right, white represents high values and black represents low values). The top plots uses a real wavelet. Note the bumpy structure along the ridge showing how the wavelet comes into and out of phase with the signal. The bottom plots use a complex wavelet. The ridge is smooth because the real and imaginary parts are out of phase.

As a comparison, recall the Fourier transform. It too is a convolution. When the oscillatory term, $e^{-i\omega t}$, and the signal have similar shapes, the contribution at that frequency is large. When they do not, the contribution is small. Unlike the wavelet transform however, the Fourier transform compares the signal to a plane wave that stretches the full length of the signal. Thus the signal must be similar to the oscillatory term everywhere, not just in localized spots. If the signal is stationary, this is indeed true and the Fourier transform can accurately pick out frequencies. If, however, the signal is non-stationary, the signal and oscillatory term will most likely *never* line up fully. At a given frequency, the similarity will be high over time intervals where that frequency is present and low where it is not (Figure 2-5). The result (and its interpretation) is therefore not clear. All that's certain is that such a convolution cannot accurately reflect the spectral content of such a signal.

2.2 Continuous and Discrete Wavelet Transforms

As described at the end of Chapter 1, the wavelet must be scaled and translated along the time axis as the transform is calculated. This is achieved by the scale variable *a* and the translation variable *b*. If these parameters are varied continuously, the result is called the continuous wavelet transform. If the variables are discretized in a particular way, however, some surprising results occur, giving rise to the discrete wavelet transform. Though the transforms differ in only this one respect, they are often used in wildly different applications.

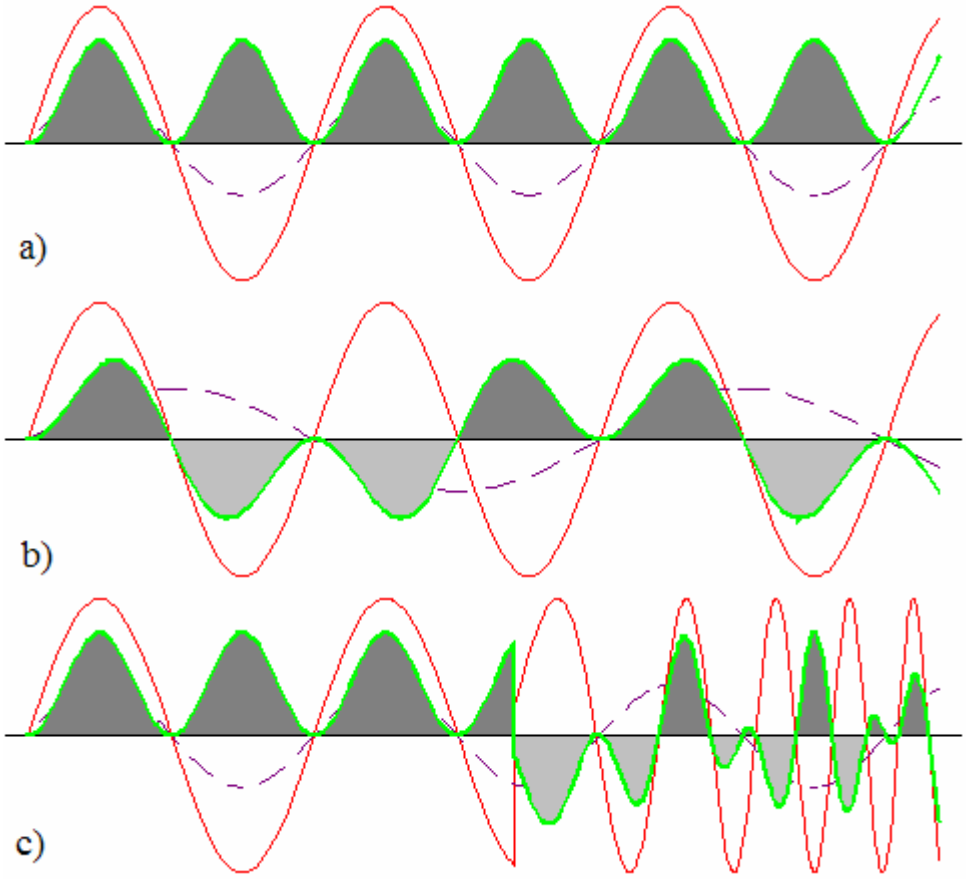

Figure 2-5: In this schematic of the Fourier transform convolution, the signal is plotted in solid red, the oscillation term is plotted in dashed purple and their product is plotted in thick green. The area beneath the product is displayed with dark grey representing positive contribution to the transform and light grey representing negative contribution.

(a) The oscillation and signal both have the same frequency. The contributions are all positive and therefore the transform result is positive.
(b) The oscillation and signal are of different frequencies. The contributions are equally positive as they are negative and therefore the result is zero.
(c) The signal is non-stationary and so the oscillation matches frequency only over a small portion. The contributions are positive over that interval, but erratic everywhere else leading to ambiguous results.

2.2.1 Daughter Wavelets

If we call the wavelet Ψ(t) the mother wavelet, the suitably scaled and translated wavelets are called daughter wavelets, ψ_{ab}. Using daughter wavelet notation, the wavelet transform can be compactly written as

$$\tilde{F}(a,b) = \int_{-\infty}^{\infty} f(t)\psi_{ab}^{*} dt \,.$$

For the continuous wavelet transform, the daughter wavelets take the form

$$\psi_{ab} = \Psi\left(\frac{t-b}{a}\right).$$

The discrete wavelet transform, on the other hand, is discretized logarithmically in a dyadic grid: $a = 2^m, b = n2^m$. Thus, daughter wavelets become

$$\psi_{mn} = \Psi\left(\frac{t-n2^m}{2^m}\right),$$

and the (formerly continuous) transform becomes a series of coefficients

$$T_{mn} = \int_{-\infty}^{\infty} f(t)\psi_{mn}(t)dt \,.$$

It is important to note that the name discrete wavelet transform refers *only* to this discretization scheme. As will be discussed below, this dyadic discretization leads to a number of important properties. If any other discretization scheme is used, the result should more properly be called a *discretized* continuous wavelet transform.

2.2.2 Discrete Wavelet Transform Usage

The dyadic discretization of the discrete wavelet transform yields two advantages. First, by using such discrete, logarithmic values for *a* and *b*, the transform can be computed very quickly[9]. Second, this choice of discretization makes it possible to use wavelets which form a complete orthogonal basis. Transforming with orthogonal wavelets means that there is no overlap in information (each transform coefficient contains information which is contained no where else) and forming a complete basis means that the coefficients together contain *all* the information. Thus, even though the wavelet is sampled discretely, an exact reconstruction of the original signal from these coefficients can be made using the inverse discrete wavelet transform. The discrete wavelet transform is an "efficient" representation in that it can represent a complex signal changing on various time scales in a small number of coefficients. In comparison, the continuous transform is said to be overcomplete. That is, it contains more information than is necessary to reconstruct the original signal.

The discrete wavelet transform enjoys extensive use in many areas, particularly digital information compression. The transform coefficients completely describe a signal, but if an approximate reconstruction will suffice, many coefficients can be thrown out to save digital storage space. Information about the signal is concentrated in the coefficients along the ridges and all other coefficients are close to zero. Therefore, if small transform coefficients are changed to zeros (which cost nothing in digital storage space), the size of the signal will be compressed without much loss in

[9] Computational algorithms exist for computing the discrete wavelet transform very efficiently; for *n* data points, there are *n* calculations. Compare this to the FFT algorithm with $n \ln(n)$ computations [14].

signal quality. The resulting coefficients can then be quickly inverse transformed when needed (Figure 2-6). This type of compression scheme is particularly utilized for images (e.g. JPEG2000 [15], [16] and SPIHT [17]) and videos (e.g. MPEG 4 [18])[10].

Figure 2-6: An image is compressed using a Fourier-based JPEG scheme (not to be confused with the wavelet-based JPEG2000) at different compression ratios in (a)-(c). The same image is compressed using the wavelet-based SPIHT scheme in (d)-(e). Note that there is almost no apparent loss in the wavelet compression even at a 64 times reduction in file size. (Source: [17].)

[10] I do not detail the 2-dimensional wavelet transform here, but the generalization from the 1-dimensional case given here is fairly straightforward. For details, consult Section 3.8 of [7].

2.2.3 *Continuous Wavelet Transform Usage*

While the special properties of the discrete wavelet transform are indeed remarkable, they are not essential for spectral estimation and in many ways can be restrictive or detrimental. Quick computation time is certainly useful, but dyadic sampling limits the time and frequency values that are examined; closely spaced frequencies or frequencies falling between scale values may be missed or blurred and fine time resolution may be compromised. Using the continuous wavelet transform with judiciously chosen discrete values of *a* and *b* gives a much better compromise between computation speed[11] and parameter choice. Being able to construct an orthonormal wavelet basis is also unnecessary for spectral estimation. No reconstruction of the original signal is performed and the wavelets that are used in such transforms are limited. Many non-orthogonal wavelets have properties that make them better suited in spectral estimation transforms. Therefore, the continuous wavelet transform is far preferable for these applications.

2.3 Wavelet *Not So* Basics

With the wavelet transform sufficiently introduced, it is now possible to focus a bit more on what makes the wavelet so powerful. Admission criteria will be addressed, followed by desirable properties and different choices for wavelets.

[11] The number of computations for *n* scales and *m* translations is *nm* ln(*m)* [19].

2.3.1 Wavelet Admissibility

To be characterized as a wavelet, a function must satisfy a number of conditions dealing with both their window and frequency aspects.

First, a wavelet must have finite energy as satisfied by the relation

$$\int_{-\infty}^{\infty} |\Psi(t)|^2 dt < \infty .$$

This condition forces the wavelet to tend toward zero as t approaches $\pm\infty$, making it a localized *wavelet* instead of an infinite *wave*. A wavelet is said to have compact support if it is zero outside a finite interval [13]. A more restrictive form of this condition requires the wavelet to be normalized:

$$\int_{-\infty}^{\infty} |\Psi(t)|^2 dt = 1 .$$

Though not strictly necessary for wavelet admissibility, normalization has become a standard condition; any wavelet which has finite energy can be scaled by a prefactor to achieve normalization.

Secondly, the wavelet must satisfy what is known as the admissibility condition[12]

$$\int_{0}^{\infty} \frac{\left|\hat{\Psi}(\omega)\right|^2}{\omega} = C_\Psi < \infty ,$$

where $\hat{\Psi}(\omega)$ is the Fourier transform of the wavelet and C_Ψ is a finite number called the admissibility constant. A wavelet meeting the admissibility condition has zero

[12] The naming is unfortunate. It is not the only condition which *admits* a wavelet, nor is it necessarily the most important. However, this is the traditional nomenclature.

mean (i.e., it sweeps out as much area above the axis as below it) which implies that there is no zero frequency component (i.e., $\hat{\Psi}(0) = 0$).

Satisfying the admissibility condition also ensures that the transform is invertible. That is, the original signal can be reconstructed from the transformed signal. Though reconstruction is not a concern in spectral estimation, invertibility does imply that the transformed signal completely characterizes the spectral content of the original signal. The inverse continuous wavelet transform is given by

$$f(t) = \frac{1}{C_\Psi} \int_{-\infty}^{\infty} \int_{-\infty}^{\infty} \tilde{F}(a,b) \psi_{ab} \frac{da db}{a^2}.$$

Formulas also exist to perform the inverse using a different wavelet than was used in the original transform [13]. Discrete wavelet transform inversion, however, requires use of the same wavelet [20].

2.3.2 Desirable Wavelet Properties

Any function which meets the conditions described above in Section 2.3.1 can be used as a wavelet, but not all wavelets work equally well in all cases. There are several properties that are desirable depending if one is using the discrete or the continuous wavelet transform. In particular, there are some properties which are useful especially for spectral estimation.

In the discrete wavelet transform case, the goals are quick computation and efficient compression. To utilize the efficient quick transform scheme, wavelets must

possess compact support (i.e., be zero outside a finite interval) and to be invertible they must be orthogonal. That is

$$\int \psi_{mn}(t)\psi^{*}_{m'n'}(t)dt = 0 \text{ if } m \neq m' \text{ and } n \neq n'.$$

To increase the compression rates of data, there are additional desirable properties. Wavelets which are either symmetric or antisymmetric better concentrate the coefficients around the ridge and produce less visual distortion in the reconstructed signal [14]. Wavelets also should be real-valued; complex wavelets will transform *n* real data points into *n* complex data points requiring twice as much storage space.

Desirable properties for wavelets used in the continuous transform are a bit different from those just discussed. Because compression and quick computation are not concerns, a wider range of options is available. Principally, wavelets should be complex-valued so that the wavelet transform plots have smooth ridges to adequately describe amplitude changes. Also, a wavelet should have no negative frequencies in its Fourier transform. To understand this, recall that real functions have Fourier transforms which are symmetric about zero. If a complex wavelet has a symmetric, or near symmetric Fourier transform, it can behave similarly to a real-valued wavelet and produce bumps in its transform ridges. Therefore, wavelets without negative frequency components minimize this problem.

When doing spectral estimation, there is also one more desirable property. A wavelet should have good time-frequency uncertainty, $\Delta t \Delta \omega$, to improve the overall

resolution of the transform plot[13]. Optimal time-frequency uncertainty is attained by a Gaussian curve, but a simple Gaussian does not satisfy the admissibility condition. Modified Gaussian wavelets, though, can be constructed to give close to optimal uncertainties. Some wavelets have tunable parameters that allow a trade off between better time or frequency resolution, and this is also highly advantageous.

2.3.3 Common Wavelets

A number of wavelets are common to the field. The main division is between those which are real and those which are complex.

For real-valued wavelets, the simplest is the Harr wavelet, given as a step function of the form

$$\Psi(t) = \begin{cases} 1 & 0 \le t < \frac{1}{2} \\ -1 & \frac{1}{2} \le t < 1 \\ 0 & otherwise \end{cases} .$$

The Harr wavelet is often used in discrete wavelet transforms because it is the only wavelet to satisfy all the desirable properties listed in Section 2.3.2; it is real, orthogonal, symmetric, and has compact support [14]. However, because it is real, it is not useful for spectral estimation. It is plotted in Figure 2-7.

[13] Recall that the time and frequency resolutions are the standard deviations of (respectively) the modulus squared wavelet and the modulus squared Fourier transformed wavelet.

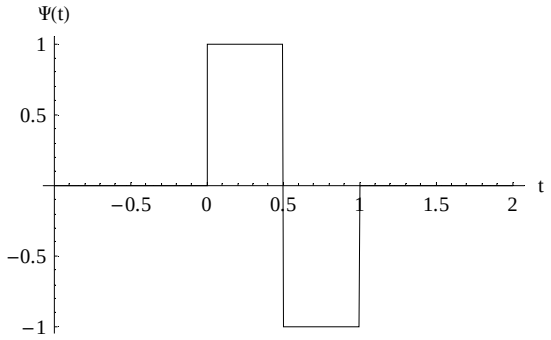

Figure 2-7: The Harr wavelet.

Another set of frequently encountered real wavelets is the group of Hermitian wavelets. These wavelets are the normalized derivatives of Gaussian curves and take the form

$$\Psi_n(t) = (2n)^{-\frac{n}{2}} c_n H_n\left(\frac{t}{\sqrt{2n}}\right)\exp\left(-\frac{t^2}{2n}\right),$$

where n corresponds to the nth derivative, H_n is the nth Hermite polynomial and c_n is the normalization constant, determined by [14] to be

$$c_n = \left(n^{\frac{1}{2}-n}\Gamma(n+\tfrac{1}{2})\right)^{-\frac{1}{2}}.$$

Of these wavelets, the most popular is the Mexican hat[14] (or Marr) wavelet corresponding to *n=2* (second derivative). Examples are plotted in Figure 2-8.

[14] ¡Viva la convolución!

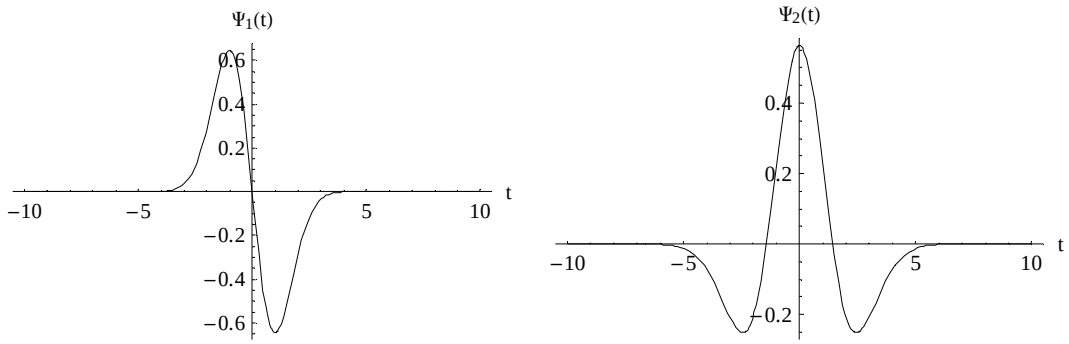

Figure 2-8: Hermitian wavelets with *n*=1 (left) and *n*=2 (Mexican hat, right).

Again, as real wavelets, these are not optimal for spectral estimation. However, such wavelets do have practical uses in other fields such as fractal and multifractal analysis [21] and singularity and edge detection [22], [23], [7].

The Hermitian wavelets can be made into complex-valued wavelets by assigning Gaussian derivatives of different order to the real and imaginary parts. Take, for example, the Hermitian hat wavelet having a real part corresponding to the second derivative and an imaginary part corresponding to the first derivative:

$$\Psi(t) = \frac{2}{\sqrt{5}}\pi^{-\frac{1}{4}}(1 - t^2 + it)\exp(-\tfrac{1}{2}t^2).$$

While the Hermitian hat wavelet is complex, it does have negative frequency components in its Fourier transform. Recall from Section 2.3.2 that negative frequencies in complex wavelets produce phase dependence problems analogous to real-valued wavelets. Thus, its use for spectral estimation is possible, but limited. The Hermitian hat wavelet has been used successfully, though, in the calculation of derivatives in the presence of noise [24]. The wavelet and its frequency spectrum are plotted in Figure 2-9.

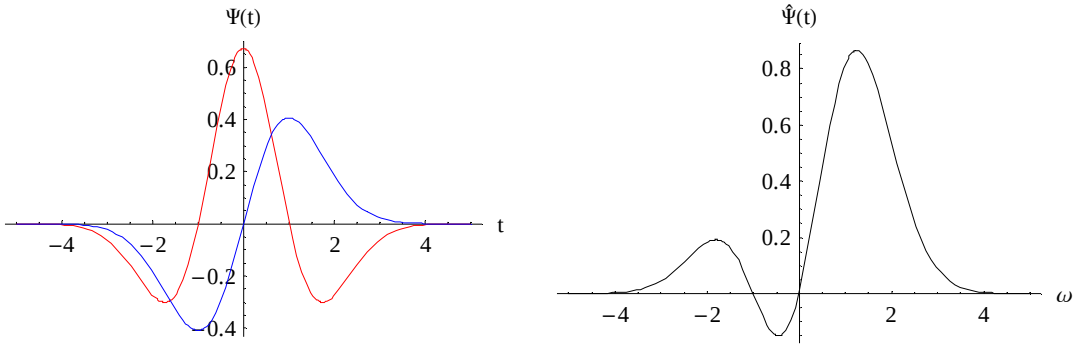

Figure 2-9: The Hermitian hat wavelet with the real part plotted in red and the imaginary part plotted in blue (left) and its Fourier transform (right).

Another complex-valued wavelet is the Paul wavelet given by

$$\Psi_m(t) = \frac{2^m i^m m!}{\sqrt{\pi(2m)!}}(1-it)^{-(m+1)},$$

where *m* is called the *order* and can be any integer value. The Paul wavelet has very quick time decay which increases with *m*; therefore, it has excellent time resolution. The downside, however, is that the frequency resolution is correspondingly poor [25]. Examples are Paul wavelets of different order are given in Figure 2-10.

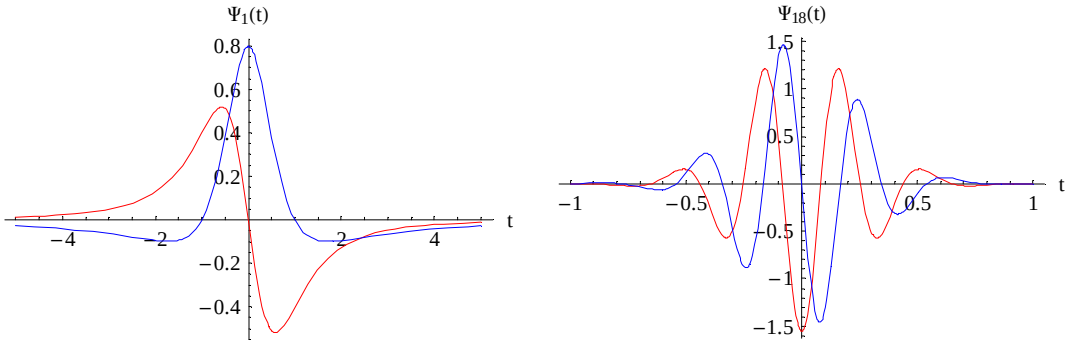

Figure 2-10: Paul wavelets of order *m*=1 (left) and *m*=18 (right) with the real part plotted in red and the imaginary part plotted in blue.

Finally, the Morlet wavelet, perhaps the most common complex-valued wavelet, is given by

$$\Psi_\sigma(t) = c_\sigma \pi^{-\frac{1}{4}} \exp(-\tfrac{1}{2}t^2)[\exp(i\sigma t) - \kappa_\sigma],$$

where the two constants are the normalization constant,

$$c_\sigma = [1 + \exp(-\sigma^2) - 2\exp(-\tfrac{3}{4}\sigma^2)]^{-\frac{1}{2}},$$

and the offset constant (which adjusts the wavelet to give it zero temporal mean and therefore satisfy the admissibility condition),

$$\kappa_\sigma = \exp(-\tfrac{1}{2}\sigma^2).$$

Any positive, non-zero, real value can be used for the parameter σ. Note from its form that the Morlet wavelet is approximately a Gaussian multiplied by a plane wave. It is plotted in Figure 2-11 for two values of σ.

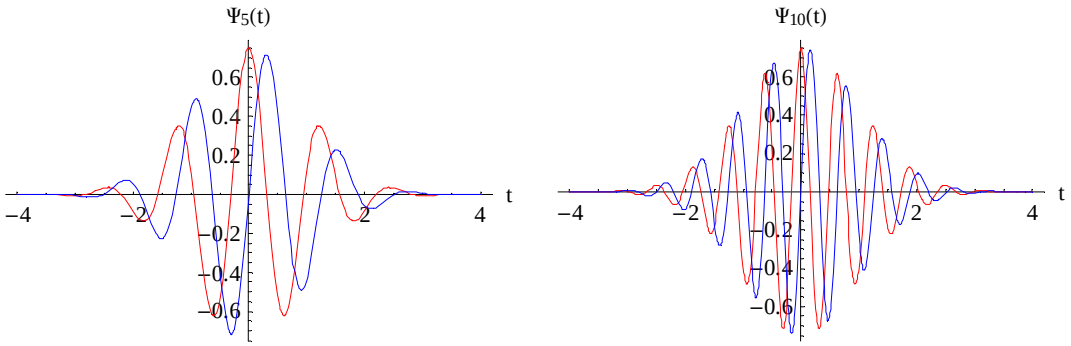

Figure 2-11: Morlet wavelets for σ=5 (left) and σ=10 (right) with the real parts plotted in red and the imaginary parts plotted in blue.

Its near-Gaussian form gives it good time-frequency uncertainty and the parameter σ allows the time and frequency resolution of the wavelet to be adjusted.

Higher values of σ give better frequency resolution and lower values give better time resolution. If $\sigma > 5$ is used, then $\kappa_\sigma < 10^{-5}$ and can be neglected with little error [7].

Despite these desirable properties, the range over which the Morlet wavelet parameter σ may be "successfully" varied is in many cases restrictive. Small values of σ cause the real part to dominate the imaginary part leading to the bumpy transform plots similar to those produced by real-valued wavelets. Large values of σ lead to such poor temporal resolution as to create ridge discontinuities and significantly lower than expected ridge amplitudes [14], [10].

2.4 Transform *Not So* Basics

Up to this point, it has sufficed to say that a plot of the wavelet transform is a mathematical representation of the signal where the locations of local maxima (ridges) give an estimate of the frequency content of a signal as a function of time. This section will give support for this claim and provide the mathematical rigor necessary to place the transform on firm theoretical ground, allowing us to proceed with confidence in the implementation and interpretation of the technique.

2.4.1 Ridges

Before addressing the wavelet *ridge*, it is instructive to return to the idea of the Fourier *peak*. It is well known and usually taken for granted that a peak in a Fourier periodogram represents a frequency present in the signal. However intuitive this may seem, a mathematical justification must exist. Such justification comes (in one format,

at least) in [3]. Using Bayesian spectral estimation techniques (outlined in Section 1.3.1), the Fourier transform is derived with purely statistical means as the probability of a single frequency in the presence of noise. Thus, a plot of this probability (equal to the Fourier plot) is peaked at the most probable frequency.

As the Fourier peak revealed the spectral content, so must the wavelet ridge, it was therefore assumed. However, justification for this interpretation did not appear until 1992 in a publication by N. Delprat *et al.* [1], with subsequent refinement added by [26], [27], and [28].

The justification is summarized as follows[15]. Any signal to be analyzed can be written in complex form, $f(t) = A_f(t)e^{i\varphi_f(t)}$ and any wavelet can be likewise expressed, $\psi(t,a,b) = A_\psi(t,a,b)e^{i\varphi_\psi(t,a,b)}$. Assuming that changes in signal amplitude are small compared to the frequency[16], that is

$$\left|\frac{1}{A}\frac{dA}{dt}\right| << \left|\frac{d\Phi}{dt}\right|,$$

the wavelet transform can be written as

$$\tilde{F}(a,b) = \tfrac{1}{2}\int_{-\infty}^{\infty} \exp[\ln(A) + i\Phi]dt\,,$$

where $A = A_f A_\psi$ and $\Phi = \varphi_f - \varphi_\psi$. The greatest contributions to the wavelet transform occur at times of stationary phase, $\Phi'(t,a,b) = 0,$ so an asymptotic

[15] For a more detailed treatment, see the in-depth summary in [14] or the original paper, [1].
[16] This assumption is justified, asserts [1], because the physical interpretation of a wave whose amplitude oscillates as fast as or faster than the frequency is inherently ambiguous and unnatural.

expansion is performed around these points. The result is that the transform is peaked when the frequency of the daughter wavelet[17] is equal to the frequency of the signal.

N. Delprat *et al.* and subsequent papers show that these results are also applicable to signals with multiple frequencies. Therefore, a signal's spectral content is completely characterized by the collection of ridges (called the skeleton [1]).

2.4.2 The Scalogram

Now that it has been established that the ridges contain the spectral information, it is left to plot the transform. The most common option is to graph the modulus with the resulting plot called the scalogram. Other plotting options (e.g., the real or imaginary parts or the phase) do not tend to be as helpful in spectral estimation[18]. In conventional 3D plotting, the parameters a and b are plotted along the x and y-axes while the value of the function is plotted along the z-axis. Alternately, the transform may be given by a contour plot.

The height of the transform plot (the z values) can be weighted to highlight different features of the scalogram or to reveal otherwise hidden ridges. For example, if ridge amplitudes differ greatly – say a strong low-oscillation frequency with a weak, high-frequency oscillation superimposed – a weighting factor such as $1/a^2$ will amplify the higher frequency components. Besides multiplying by a factor, other common techniques include plotting the logarithm or square of the modulus (Figure 2-12).

[17] See below, Section 2.4.3, for the conversion from scale to frequency.
[18] In [1], a technique is given to estimate frequency content from the phase. A subsequent paper, [26], shows that frequency estimation based on the modulus is more "robust" in the presence of noise.

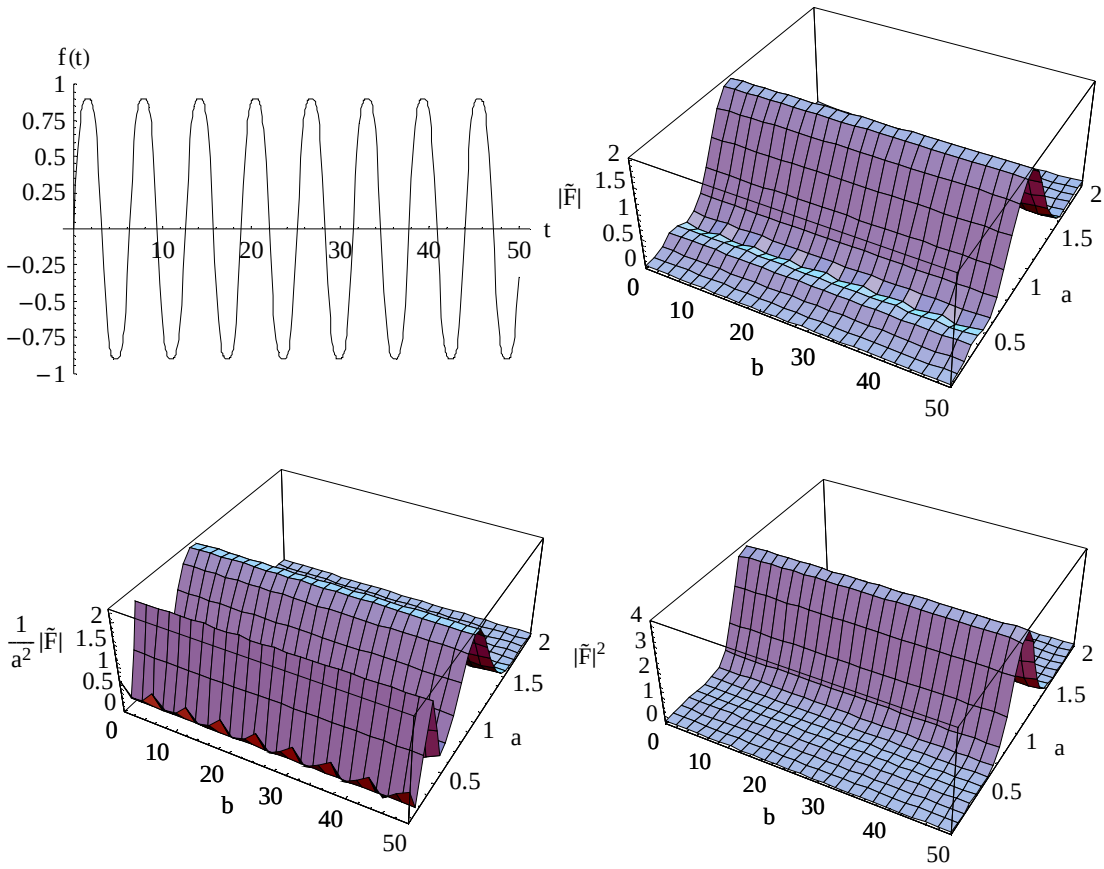

Figure 2-12: The signal $f(t)$=sin(t)+0.1sin($3t$) is plotted (top left) as is its wavelet scalogram (top right). Note the very small bump near a=0.33 representing the ω=3 frequency. Two different weighting schemes are used in the plots that follow. On the left, scaling by $1/a^2$ makes the lower a ridge grow to nearly the same height as the other ridge. In the plot on the right, squaring the modulus makes the ridge essentially disappear.

2.4.3 Time-Frequency Representation

The scalogram can in many ways be regarded as a *qualitative* picture of the spectral content of a signal. The ridges reveal the presence, relative strength and time relation of signal components, but do not attach definite, relevant values to these quantities. Though correct and potentially informative, a more *quantitative* result that replaces the translation and scale parameters and the modulus height with the more conventional (and easy to understand) quantities of frequency, time and amplitude is

desired. With such conversions, the scalogram is elevated to the more useful time-frequency representation.

First, conversion from the translation parameter to time is simple. Because the mother wavelet is defined so that it is centered at time *t=0*, the translation of the daughter wavelets by the replacement $t \to t - b$ means that the daughter wavelets are centered at time *t=b*. The center of the convolution between wavelet and signal is the center of the wavelet, so the transform result reflects the behavior of the signal at that center. Thus the conversion from translation to time is the simple substitution *t = b*.

Next is the conversion from scale parameter *a* to frequency ω. Recall that scale is a direct measurement of the "width" of the wavelet window; increasing *a* increases the width, and therefore the period, of the wavelet. It follows then, that as *a* is increased, the corresponding wavelet oscillation frequency is decreased: $\omega \propto 1/a$. Because the width of the wavelet is defined differently for each mother wavelet, the proportionality between scale and frequency is also different. This proportionality constant is the central frequency of the wavelet, ω_ψ, defined as the global maximum of the Fourier transform. Therefore, $\omega = \frac{\omega_\psi}{a}$.

Finally, the conversion between modulus and amplitude is achieved by returning to the approximations of N. Delprat *et al.* that were given for the justification of the ridge (Section 2.4.1). Recall that the transform was peaked at points of stationary phase, $\Phi'(t,a,b) = 0$ which corresponds to $a\phi_f = \omega_\psi$. In this region, the modulus of the transform is approximately

$$\left|\tilde{F}(a,b)\right| = \sqrt{\sqrt{\tfrac{\pi}{2}}\sigma_\psi}\, A_f(b)$$

where σ_ψ is the approximate Gaussian width of the wavelet [14]. Therefore, the amplitude of the signal is given by

$$A_f(b) = (\tfrac{1}{2}\pi\sigma_\psi^2)^{-1/4}\left|\tilde{F}(a,b)\right|.$$

Chapter 3 Methods and Techniques

The previous chapter gave a general overview of the continuous wavelet transform. This chapter will address its implementation and interpretation. Here, I discuss our choice of wavelet and our methods for transform computation as well as detail some frequently neglected, yet important, aspects of proper transform interpretation as applied to these choices.

3.1 The Hilbert-Hermitian Wavelet

Desirable wavelet properties were discussed in Section 2.3.2 and in Section 2.3.3 a number of common wavelets were presented. From this information, the best choice of wavelet for spectral estimation is arguably the Morlet wavelet as it is complex-valued, possesses tunable time and frequency resolutions, and has good time-frequency uncertainty. Recall though, that the wavelet has faults as well, primarily that small or large values of σ give unacceptable transforms. In an effort to rectify these problems, several new wavelets were created by J. Harrop [14] to bring out the wavelet properties desirable for spectral estimation. Among them, the Hilbert-

Hermitian wavelet is considered the best improvement and therefore is the wavelet we have chosen to use for our work.

The Hilbert-Hermitian wavelet is defined not in time space, but in frequency space as a Fourier transform

$$\hat{\Psi}_\sigma(\omega) = \begin{cases} c_\sigma \omega^\sigma \exp(-\frac{1}{2}\sigma\omega^2) & \omega \geq 0 \\ 0 & \omega \leq 0 \end{cases},$$

where the normalization constant is given by

$$c_\sigma = \sqrt{2}[\sigma^{-(\sigma+\frac{1}{2})}\Gamma(\sigma+\frac{1}{2})]$$

for any real, positive value of σ. Temporally, the wavelet resembles the Hermitian wavelets, however, it is complex-valued and has the parameter σ which adjusts the time and frequency resolutions like the Morlet wavelet. A plot of the wavelet in time space is given in Figure 3-1.

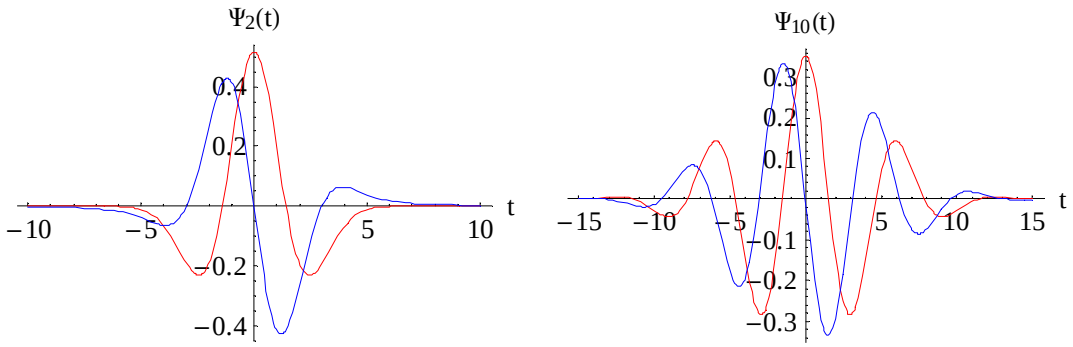

Figure 3-1: The Hilbert-Hermitian Wavelet for σ=2 (left) and σ=10 (right) with the real part plotted in red and the imaginary part plotted in blue.

This wavelet has (by construction) many advantages. It has low overall time-frequency uncertainty (comparable to that of the near-optimal Morlet) and has time and frequency resolution tunability over a wide range without problems (allowing high

temporal localization if desired). Additionally, the wavelet has a central frequency of $\omega_0 = 1$ which simplifies the conversion from scale to frequency.

3.2 Computation

The wavelet transform can be computed using any computer algorithm for integration or there are several commercial and free programs available dealing specifically with wavelet transforms. Several computer algebra systems have also released add-ons to their programs such as *Wavelet Toolbox* for *MATLAB* and *Wavelet Explorer* for *Mathematica*.

For our studies, we chose to use the *Mathematica* add-on package *Time-Frequency Analysis*[19] available from Flying Frog Consultancy for several reasons [29]. First, the package uses the Hilbert-Hermitian wavelet described above and has been successfully applied to numerous spectral estimation problems [31], [32]. Second, the *Mathematica* computing environment provides a number of beneficial features such as ease of use, simple import and export of data files, and built-in functions for 2D and 3D graphing, statistical analysis, Fourier analysis, and optimization.

The add-on package computes an approximation to the continuous wavelet transform at discretely sampled values of scale and translation producing a matrix of values that can be easily plotted in 3D or contour. The package also can perform the necessary conversions to produce the time-frequency representation displaying signal amplitude as a function of time and frequency. The discretization and range of the

[19] This package was originally developed in conjunction with [14].

transform is controlled and the parameter σ is varied by supplying options to *Mathematica* commands. The literature accompanying the package [30] explains that the computation time for a transform of approximately 1000 time steps is about 1 minute on a 1GHz desktop processor. Many of our analyses utilized significantly more time steps (approximately 4000) and were run on a faster machine (2.5GHz) taking just under 9 minutes to compute.

3.3 Ridge Extraction

As the section 2.4.1 explained, the time-frequency information of a signal is characterized completely by the ridges of the transform plot. Therefore, the ultimate goal of our analysis is to extract a trace of the skeleton of the plot.

Because the ridge is the local maximum of the function, any numerical optimization routine can be used. In our case, *Mathematica's* built-in "FindMax" function works well. Techniques have also been invented specifically for culling ridges from wavelet transforms of signals with high levels of noise, particularly the "Crazy Climber Algorithm" [27] and "Snake Penalization" [26]. Thus, the location of the extracted ridge can be equated to the signal's frequency, $\omega(t)$, and the height of the ridge equated to its amplitude, $A(t)$. These extracted functions are easily plotted in two dimensions as in Figure 3-2.

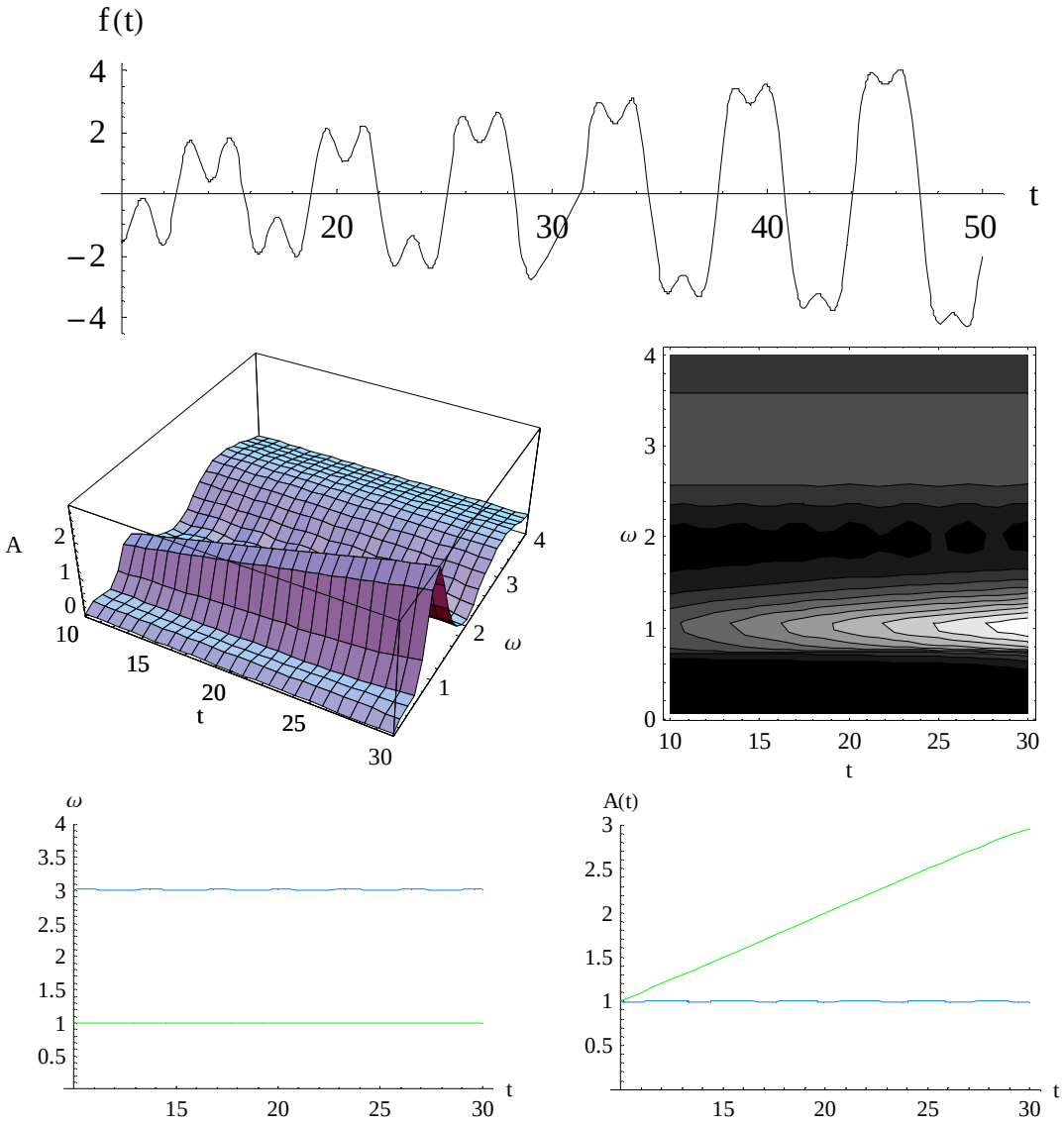

Figure 3-2: The non-stationary signal $f(t) = \frac{t}{10}\sin(t) + \sin(3t)$ is plotted (top) and wavelet transformed with the 3D and contour time-frequency representations shown (middle left and right). The extracted frequency and amplitude (bottom left and right) match the signal well.

3.4 Statistical Treatment

Most interpretations of the wavelet transform stop with the plotting of the time-frequency representation or the extraction of the ridges. However, some situations call for a bit more treatment to ensure proper interpretation. During our

studies of the wavelet transform, we identified two oft neglected points: cone of influence identification and confidence level determination. Both of these have been addressed only sporadically in papers, with in-depth treatment found only in the seminal “A practical guide to Wavelet Analysis” from C. Torrence and G. Compo [20]. Additionally, neither of these considerations was addressed in the original formation of the Hilbert-Hermitian wavelet. We have therefore investigated how to incorporate these points into interpretations of our plots which use this wavelet.

3.4.1 Cone of Influence

Recall the basic action of the wavelet transform. At each time step along the translation of the wavelet, the wavelet and signal are multiplied and the result integrated *over all t.* Because the wavelet is localized however, this integral over all *t* is actually only an integral over the width of the wavelet; beyond a certain point, the wavelet is essentially zero and the resulting product and integral are negligible. Therefore, the fact that a time series is finite is usually not important; the information at times before and after the wavelet don’t factor into the result. However, when performing the transform near one of the ends of the data, some of the wavelet overlaps where no data exists.

What happens in this case depends on how the transform is numerically formulated. It is possible to pad either side of the data with zeros or with a constant value, to add a decay to bring the signal linearly or exponentially down to zero, to connect the ends of the data together to form a continuous loop, to add a reflection of

the signal, or to create a polynomial interpolation or extrapolation to extend the signal [7], [20]. Whatever method is used, the ultimate result is that edge effects are produced close to the ends because data involved in the calculation is not real. The area of the resulting transform in which these effects are important is called the cone of influence and all results within this area are considered unreliable. Because the width of a wavelet is determined by its scale, the area affected grows with increasing *a* hence the triangular ("cone") shape. When plotted in terms of frequency, the cone distorts because it goes as 1/*a*. An example is plotted in Figure 3-3.

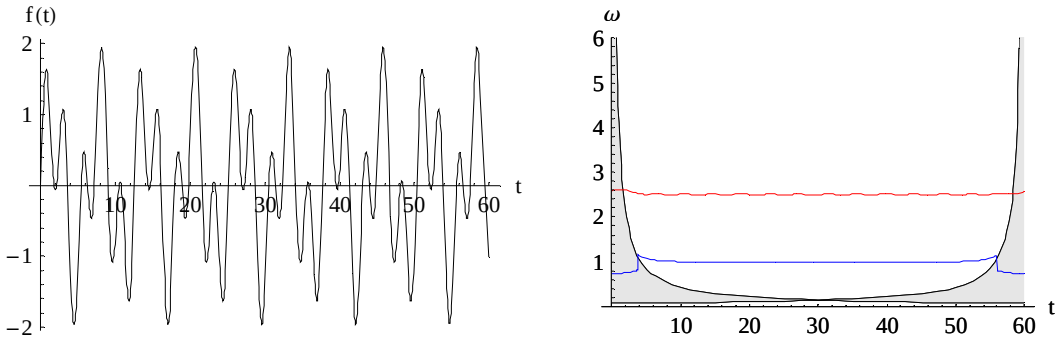

Figure 3-3: The signal *f*(t)=sin(*t*)+sin(2.5*t*) is plotted on the left. The ridges from the wavelet transform are plotted on the right, with the cone of influence shown.

Torrence and Compo explain that the width of the cone of influence is determined by the e-folding time [20]. The e-folding time is defined as the time it takes for the modulus of the transform of a signal discontinuity to decay by a factor of 1/*e*. That is, for any discontinuous signal, the transform will have a vertical ridge along all values of scale (frequency) at the time of the discontinuity that falls off by 1/*e* an e-folding time away (Figure 3-4).

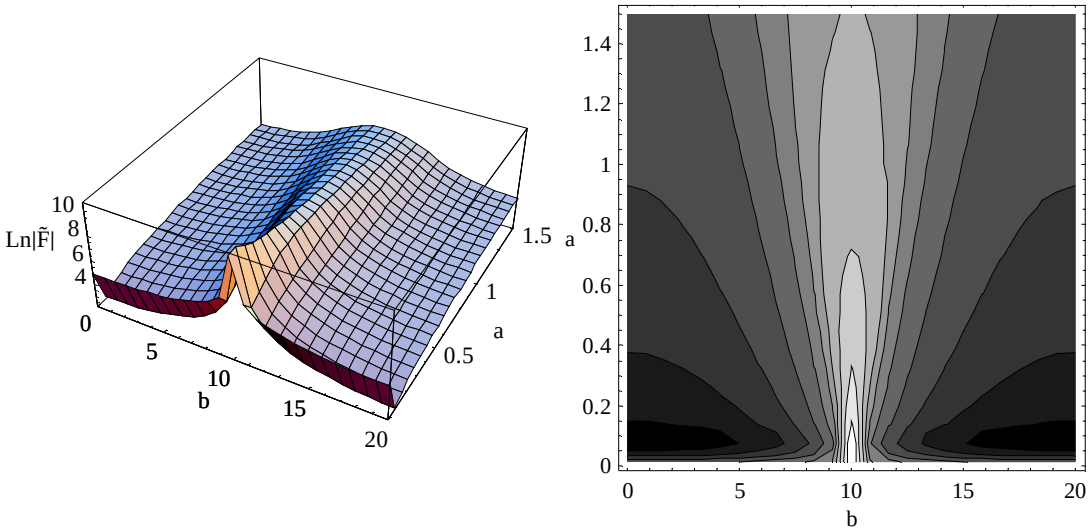

Figure 3-4: A discontinuous signal (a delta function, not shown) creates a ridge in the time direction in the wavelet transform from which the e-folding time can be computed. Note how the ridge broadens with increasing *a*.

Our analyses use the Hilbert-Hermitian wavelet, but no e-folding time information was provided by its creator. However, retracing the derivation of the wavelet shows that because its form is based closely on the family of Hermitian wavelets, its e-folding time should be similar to that family's, given as $\tau = \sqrt{2}a$ by [20]. To test this hypothesis, we generated several discontinuous signals and transformed them with the Hilbert-Hermitian wavelet. Measurements of the e-folding time were consistent with our assumption; the true e-folding time is indeed $\tau = \sqrt{2}a$.

However, we discovered that when we transformed data and applied the cone of influence, transform artifacts often appeared outside this region. The e-folding time reduces discontinuity peaks by 1/*e* (approximately 37%) which does not seem sufficient. Thus, for width of the cone of influence, we chose not to use the e-folding time, but the empirically chosen value of $\tau = 3\sqrt{2}a$ for all of our analyses. All plots

using this wavelet where data near the edge of the time series is encountered include a cone of influence of this width. If the transform is taken away from these edges, no cone of influence is needed.

3.4.2 Confidence Levels

For any experimentally generated data, inherent noise yields uncertainty. When plotting such data, one usually includes error bars or attempts to detrend out the noise. If such experimental data is transformed using Fourier or wavelet techniques, this uncertainty must be propagated as well. Therefore, any wavelet plot of an experimental signal should have some estimate of the certainty of the results. The most obvious choice for the wavelet transform is to define confidence levels. That is, 3D or contour levels for which ridges with larger amplitudes can be assumed to be real (with a corresponding percent confidence) and not due to noise in the signal.

According to Torrence and Compo, if the noise of the signal is normally distributed, then its counterpart in the wavelet modulus squared will be chi-square distributed, analogous to the Fourier transform [20]. From this, they derive the appropriate formulas for estimating noise. However, since we are working not in terms of moduli but in terms of time-frequency representations, the correspondence is clearer: for noise of variance σ^2, the distribution of noise in the time-frequency representation should also have variance σ^2. Normal statistical methods for linking standard deviation to confidence therefore apply. For example, a confidence level of

about 67% can be placed at a height one standard deviation above the noise mean or a confidence level of about 95% confidence at two standard deviations.

If an estimate of the noise is not known prior to computing the transform, one can be made from the transform results. In the raw signal, noise can be thought of as simply additional frequency components superimposed onto the data of relevance. Transforming the signal will then reveal ridges along the frequencies of interest as well as non-zero "fuzz" at large frequency values produced by the noise (Figure 3-5). Estimating the amplitude or variance of this fuzz gives a reasonable estimate of the noise in the signal [33][20].

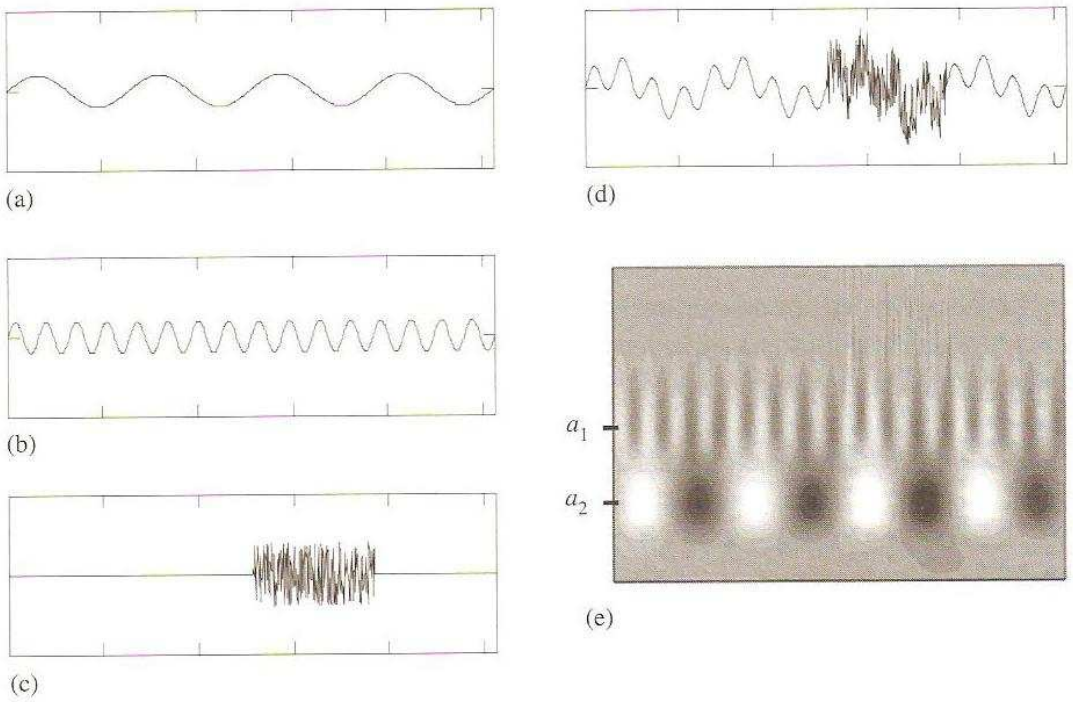

Figure 3-5: The signal plotted in (d) is a composite of (a)-(c). Note the high frequency fuzz created by the noise. (Source: [7].)

[20] One needs to be careful here. A complete investigation of how to treat and estimate noise is beyond the scope of this thesis. The technique described here enjoys general usage (e.g. [7], [33]), but the high frequency fuzz may not completely characterize the noise in all cases (e.g. frequency dependent noise).

Once appropriate levels are determined, they are usually displayed as different shadings on a contour plot, or as error bars on the extracted ridge.

Chapter 4 Applications

With the theory established, it is time to begin using the wavelet transform. We first test our techniques with a classic time series, Wolf's relative sunspot numbers, and demonstrate that our methods can produce results matching those of the current literature. The rest of the chapter is devoted to an interesting application of wavelets to the study of energy transfer in molecular dynamics simulations.

4.1 Wolf's Relative Sunspot Numbers

One of the most studied and storied classic time series is Wolf's relative sunspot numbers. This measurement, conceived by Rudolf Wolf in 1849, is computed as

$$R=k(10g+s)$$

where s is the number of individual sunspots, g is the number of group sunspots and k is called the "observatory factor" and reflects the location and instrumentation used [34]. Numbers are computed yearly from 1700, monthly from 1748, and daily today [35]. The series is often averaged monthly, seasonally or annually to match the data used.

Sunspot oscillation was first observed by Heinrich Schwabe in 1843 and is usually described as an 11 year cycle [36]. However, the period of oscillation is hardly constant; variations of up to a factor of two can be seen over some intervals of time. The first investigations of the series predate most time-frequency analysis techniques[21], but over its long history the series has been analyzed extensively. Arthur Schuster looked at the cycle with his periodogram [37], many analyses with Fourier techniques have been done [38], and a thorough Bayesian spectral treatment has been applied [3]. An excellent wavelet analysis of this and other solar time series was given by Fligge, et al. [33] on which we rely heavily on in our own study. Some authors have also done cross-wavelet analyses[22] to find correlation between the sunspot cycle and monsoons [39], crop growth [40], and wind oscillations [41].

For our analysis, we chose a seasonally averaged version of the series dating from 1749 [42] which is plotted in Figure 4-1. A periodicity is apparent, but so is non-stationarity, both in frequency and amplitude.

[21] This time series also predates Joseph Fourier (1768-1830) and therefore the Fourier transform. Since this is Chapter 4, perhaps it is appropriate to digress for a moment. Fourier was made Napoleon's governor of lower Egypt after his 1798 expedition [43]. At least one person has postulated that he "may have been the idiot that allowed the Sphinx' nose to be shot off" [44].

[22] Though not detailed in our wavelet review (Chapter 2), cross-wavelet analysis compares wavelet transforms to determine correlation between time series. Further details can be found in [20].

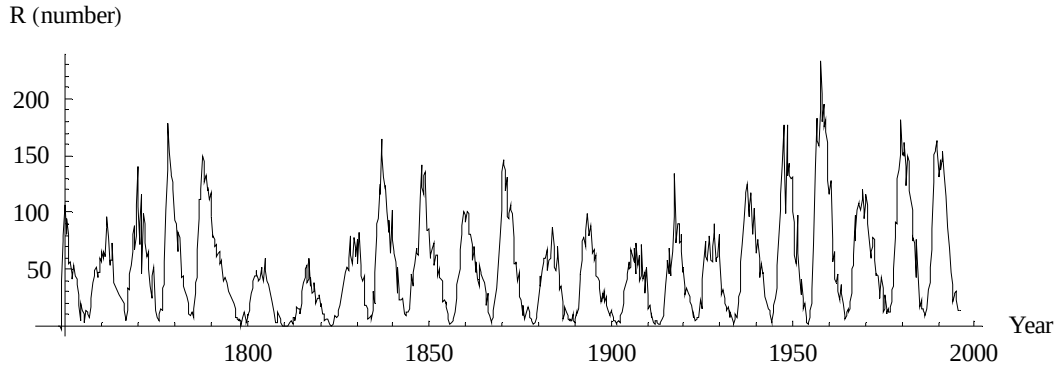

Figure 4-1: A plot of Wolf's relative sunspot numbers, seasonally averaged.

Before performing the wavelet transform, it is informative to examine the Fourier periodogram (Figure 4-2). It is easy to see that the bulk of the periodicity is indeed near T=11 years, but significant peaks surround this center at periods of 8, 9, 10, and 15 years. The plot is misleading; there is only one frequency present at any given time, but it varies continuously. When the wavelet transform is applied, the true nature is revealed. The contour plot (with confidence levels) is plotted in Figure 4-3 and the extracted frequency and amplitude are plotted in Figure 4-4.

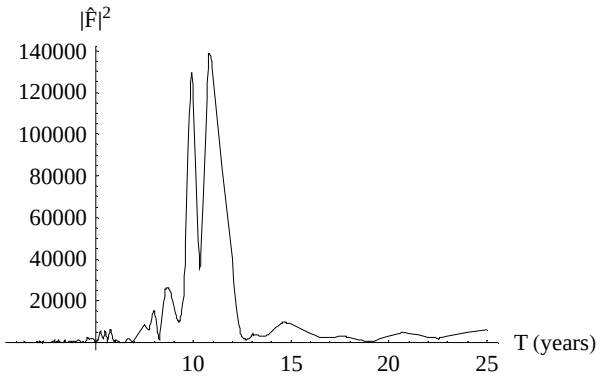

Figure 4-2: The Fourier periodogram of Wolf's relative sunspot numbers.

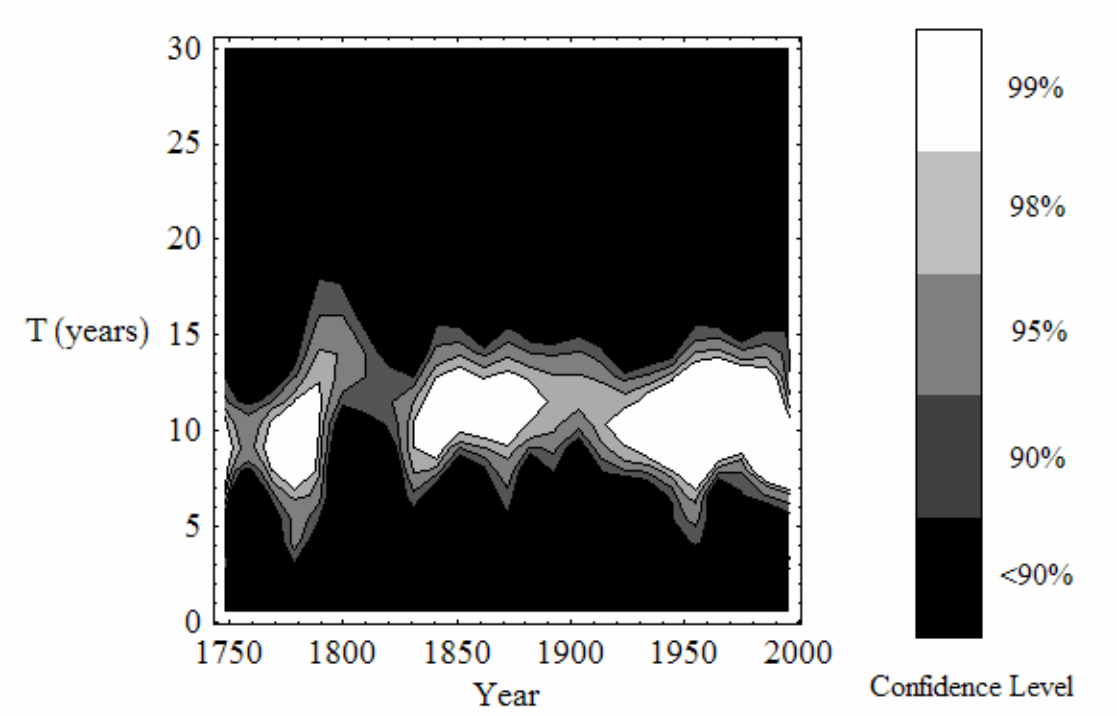

Figure 4-3: A contour plot of the wavelet transform of Wolf's relative sunspot numbers with confidence levels marked. Note that nearly the entire ridge is at or above the 98% confidence level.

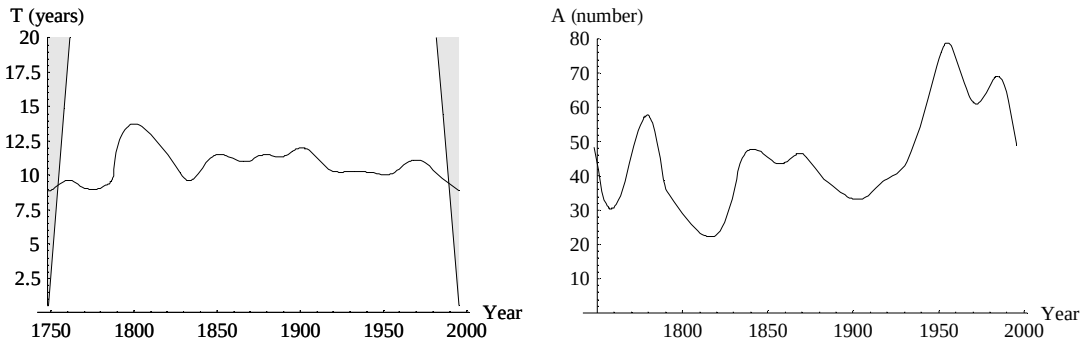

Figure 4-4: The extracted frequency (left) and amplitude (right) from the wavelet transform of Wolf's relative sunspot numbers. The grey area is the cone of influence.

Our results seem consistent with the raw data plot and with the agreed upon "average period" of 11 years, but we can go further and compare our results to the wavelet results of Fligge *et al.* mentioned before [33]. Their transform had important

differences from ours. First, they used the yearly averaged time series beginning in 1700 instead of the seasonally averaged series from 1748 that we used and, second, they used the Morlet wavelet for their analysis instead of the Hilbert-Hermitian wavelet. Their contour plot, shown in Figure 4-5, is, however, nearly identical to ours.

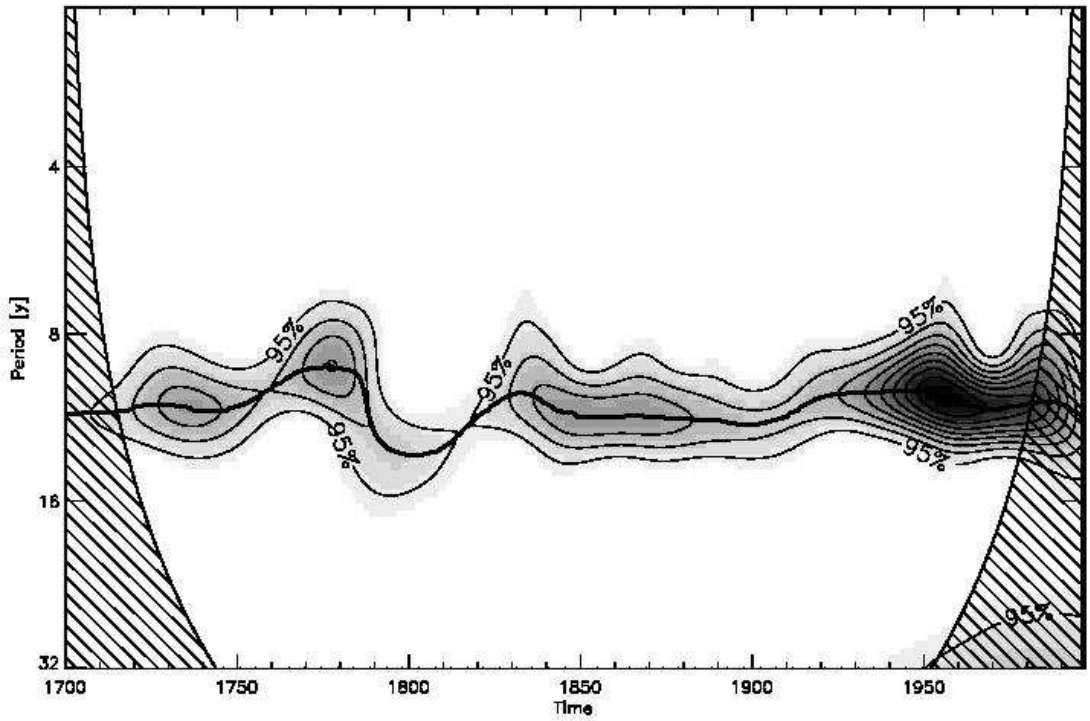

Figure 4-5: The contour plot of the wavelet transform of Wolf's relative sunspot numbers as computed by Fligge *et al.* Note that the period scale is inverted and logarithmic compared to our plot. The 95% confidence contour is marked with additional contours at successively higher confidence. Hatching marks the cone of influence. (Source: [33].)

4.2 Molecular Dynamics Simulations

With the wavelet transform and our techniques validated, we can tackle a new problem; we have chosen to study data from molecular dynamics simulations. In these simulations, atoms are arranged as molecules or in lattices and allowed to evolve over

time under various models. These simulations provide time series in the form of atom positions and velocities and we can apply the wavelet transform to this data or to derived time series such as autocorrelation functions. From these transforms, we expect to identify the frequencies of vibration between atoms and, in the case of the most complicated systems, energy transfer between modes of oscillation.

Spectral estimation like this has traditionally employed the Fourier transform. However, some aspects of the signal may be non-stationary so the wavelet transform is necessary. The study of energy transfer, for example, relies completely on signal amplitude as a function of time and so cannot be inferred from conventional techniques.

4.2.1 Energy Transfer Example: Coupled Pendulums

As a primer to our study of simulation data, it is instructive to see how energy transfer manifests itself in wavelet transforms. Consider two coupled pendulums as illustrated in Figure 4-6. If they were not connected, the two pendulums would oscillate with steady frequencies at constant amplitudes (neglecting resistance) for all time. However, the addition of the spring allows energy to flow from one bob to the other. As one oscillates with a large amplitude, the other will pull on it through the spring and reduce its amplitude. In doing so, the second pendulum increases its amplitude and eventually overtakes that of the first; the two bobs continuously exchange a fixed total energy.

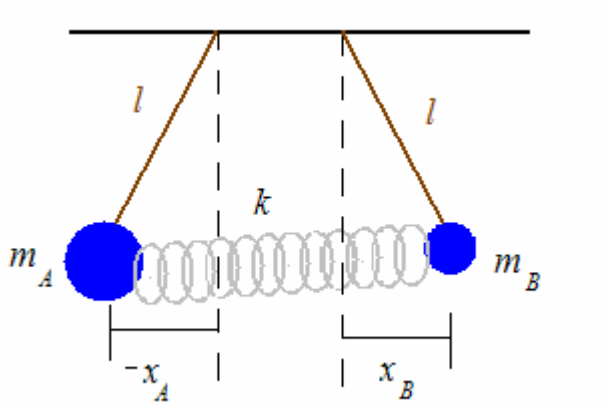

Figure 4-6: A system of coupled pendulums. Pendulum A has mass m_1=1kg and length l=1m while pendulum B has mass m_2=0.5kg and length l=1m. The spring between them has spring constant k=1N/m.

The mechanics in the relatively simple case of coupled pendulums can be completely solved analytically and the displacements of the pendulums as functions of time are plotted in Figure 4-7. From these plots, it can be seen that the pendulums oscillate at constant frequency while motion is confined to an envelope of changing amplitude.

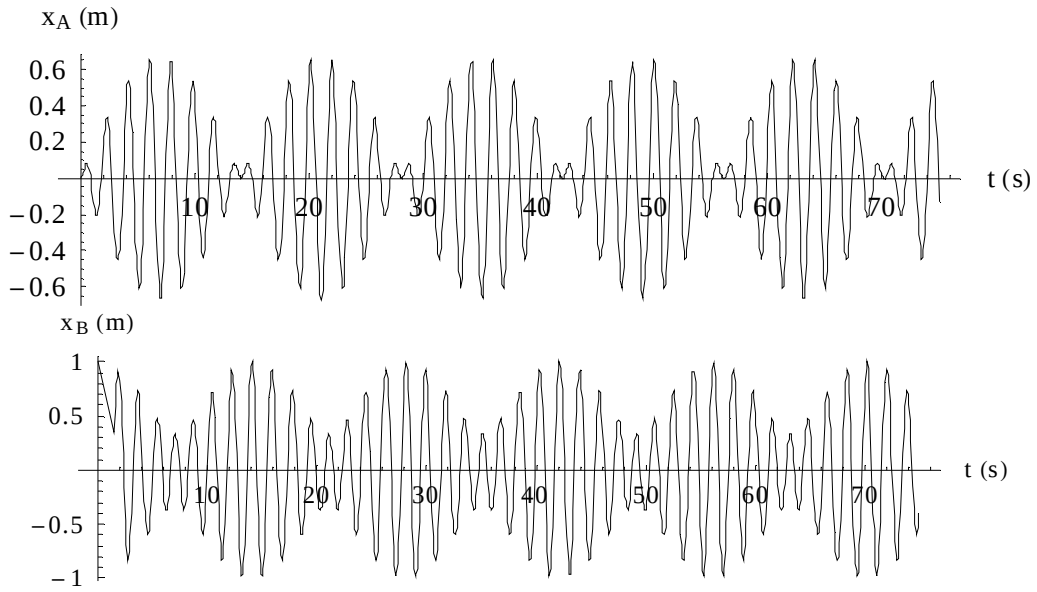

Figure 4-7: Displacement as a function of time for pendulums A (top) and B (bottom).

Performing the wavelet transform on these two position functions gives the plots seen in Figure 4-8. Here, the frequencies of oscillation on both plots form a ridge, but that ridge is not smooth and flat: it is bumpy. Unlike the bumpiness seen with real-valued wavelets, this bumpiness is not an artifact; it is the envelope that describes the changing amplitude.

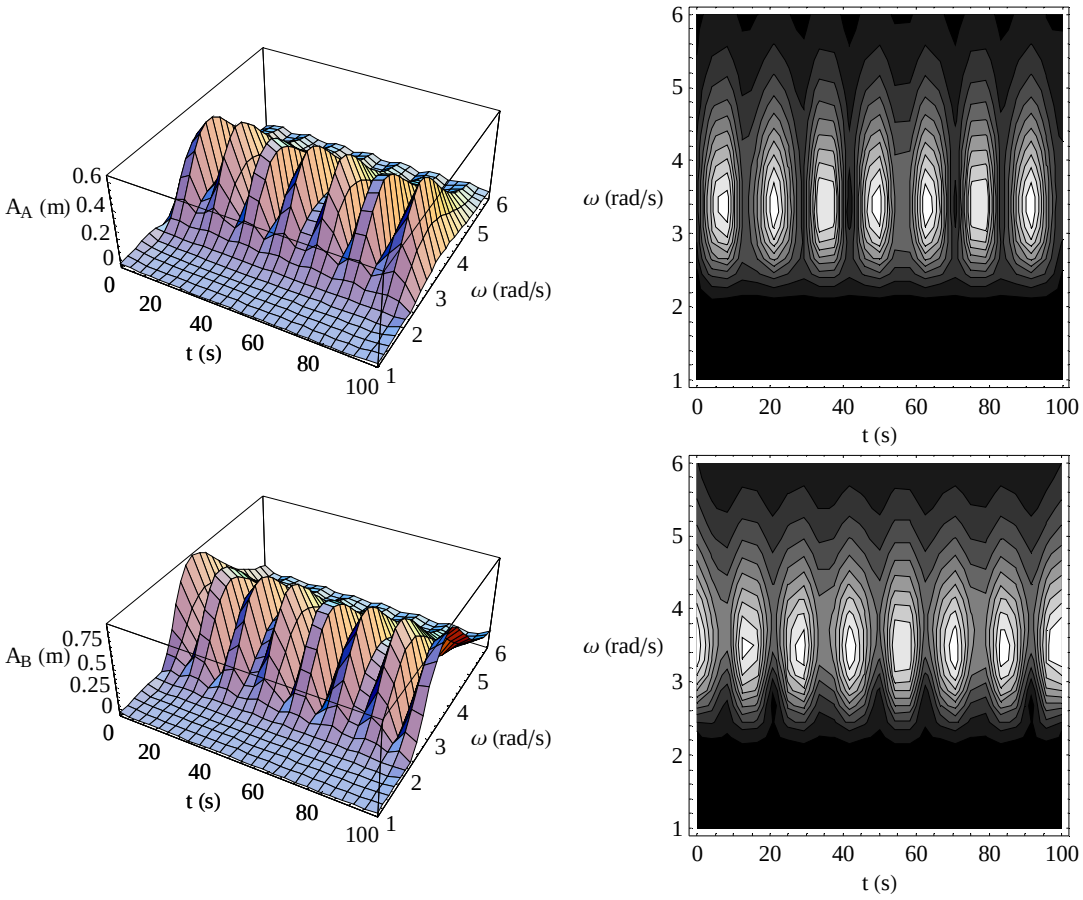

Figure 4-8: Wavelet transform of the displacement of pendulum A (top) and pendulum B (bottom).

Recall that the energy of a simple harmonic oscillator such as this is given as

$$E = \tfrac{1}{2} m\omega^2 A^2$$

where *A* is the amplitude. Extracted amplitudes and the calculated energies for each pendulum are plotted in Figure 4-9.

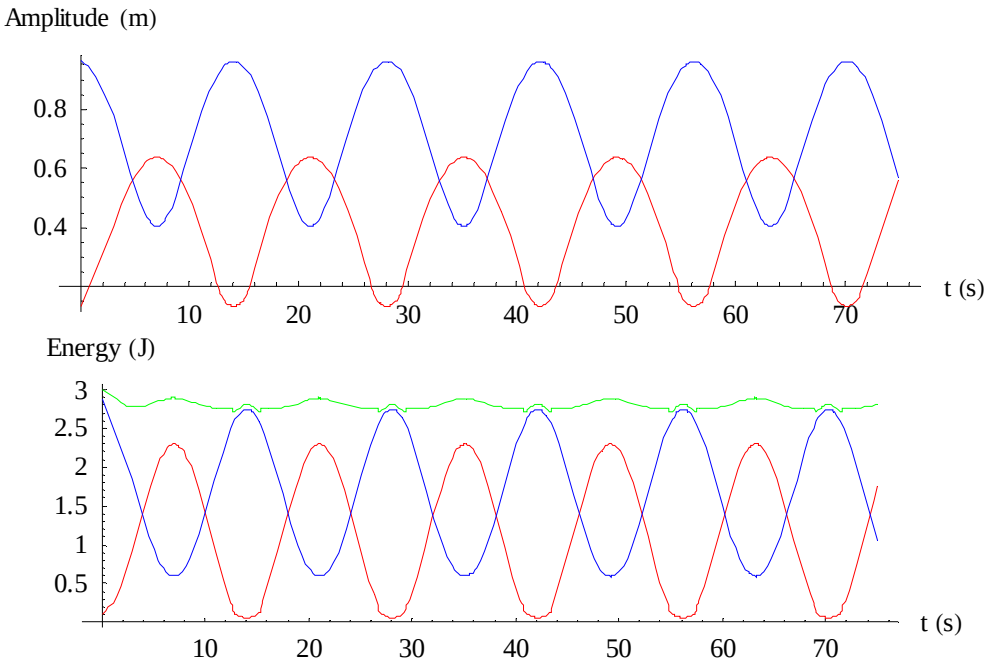

Figure 4-9: The top plot shows the extracted amplitudes of pendulum A (red) and pendulum B (blue). The bottom plot shows the calculated energy of each as well as their sum (green). The amplitudes and energies are out of phase and the total energy is constant[23].

Thus, energy transfer between two oscillation modes in a system can be seen in a wavelet transform as modulation in ridge amplitude. As energy enters one oscillation, its transform amplitude increases and as it leaves, the amplitude decreases.

[23] The total energy (green) is not exactly constant because it is difficult to extract ridges from the transform plot when they are at low amplitudes.

Detection of this time-dependent phenomenon is impossible using Fourier or other stationary signal techniques.[24]

4.2.2 Toy Model: Carbon Trimer Molecules

Before exploring a full lattice simulation, we examine a toy model of the carbon trimer molecule, C_3. This molecule forms a linear chain and its vibrational spectrum is easily interpreted in terms of longitudinal and transverse normal modes (Figure 4-10). A number of *ab initio* molecular dynamics simulations were computed (in the manner of [45]) and analyzed with the wavelet transform. They were done at various average temperatures and were in some cases begun with initial oscillation confined to specific modes. These simple models did not exhibit any non-stationary features; there was no energy transfer or frequency change. However, these models did serve as good practice before attempting the more complex system.

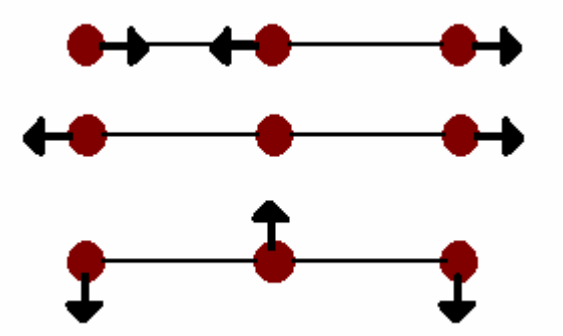

Figure 4-10: The two longitudinal and one transverse normal modes of C_3.

[24] Recall from Section 2.4.1 that the amplitude of a signal must vary much more slowly than the phase for our ridge interpretation to hold. An argument can be made here that the amplitude envelope (because it is periodic) is simply another frequency to be determined in the problem. Because of the magnitude of the difference however, the envelope appears as the amplitude. A wavelet transform of the extracted amplitude could provide the frequency of the energy transfer if desired.

The most interesting simulation is a carbon trimer at an average temperature of 3400K that was begun in its transverse mode. For all three atoms, it will suffice to look at the x-coordinate only. (The y-coordinate plots are similar.) The Fourier plots (Figure 4-11) show strong peaks at $0.0458fs^{-1}$ and $0.0935fs^{-1}$ with many smaller peaks above $0.1fs^{-1}$ for the center atom. For the two end atoms, these peaks also appear, a much stronger additional peak is present at $0.0225fs^{-1}$. Because this molecule was begun in a pure mode, there is only one normal mode frequency which is assumed to be $0.0225fs^{-1}$ because it is by far the dominant. Each of the other frequencies is an anharmonic effect. Note that each occurs at integer multiples of the principal peak.

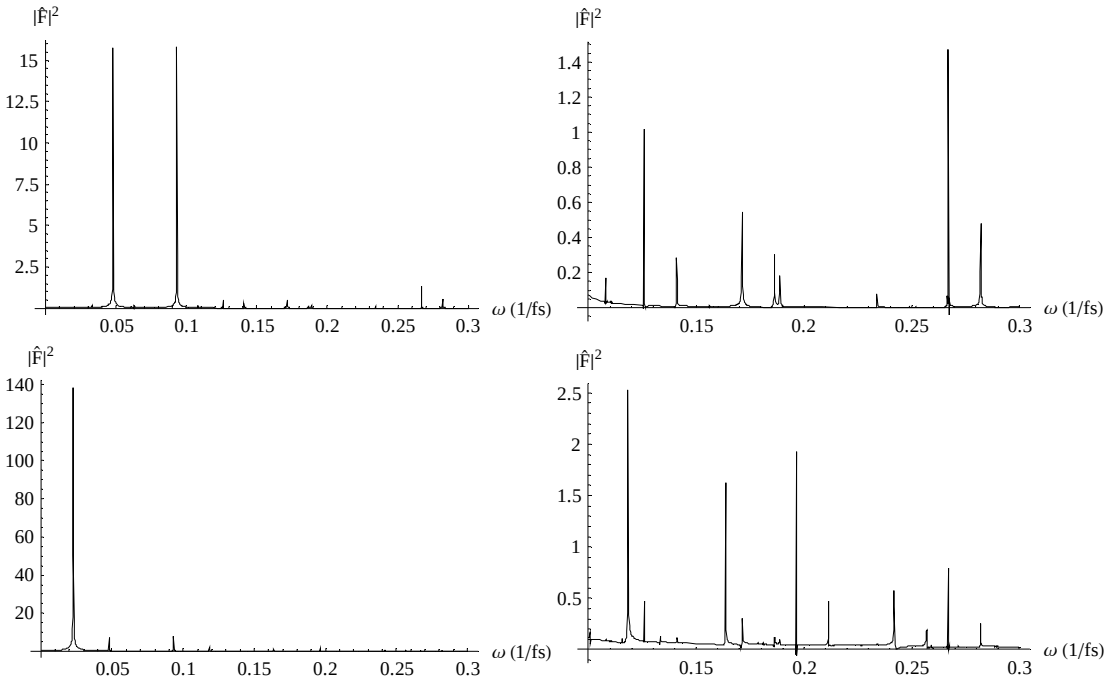

Figure 4-11: Fourier plots of the center atom (top) and the two end atoms (bottom) plotted to show different intervals. (The end atoms have identical plots, so only one is shown.)

Performing the wavelet analysis on these data series yields the plots in Figure 4-12. As expected, the dominant frequencies seen in the Fourier transform are found. Note that for the two end atoms, the principal normal mode frequency is dominant, but for the center atom, this frequency is absent. Also note that the width of the transform peak for this value partially obscures the nearest anharmonic peak; only the second anharmonic is clearly resolved.

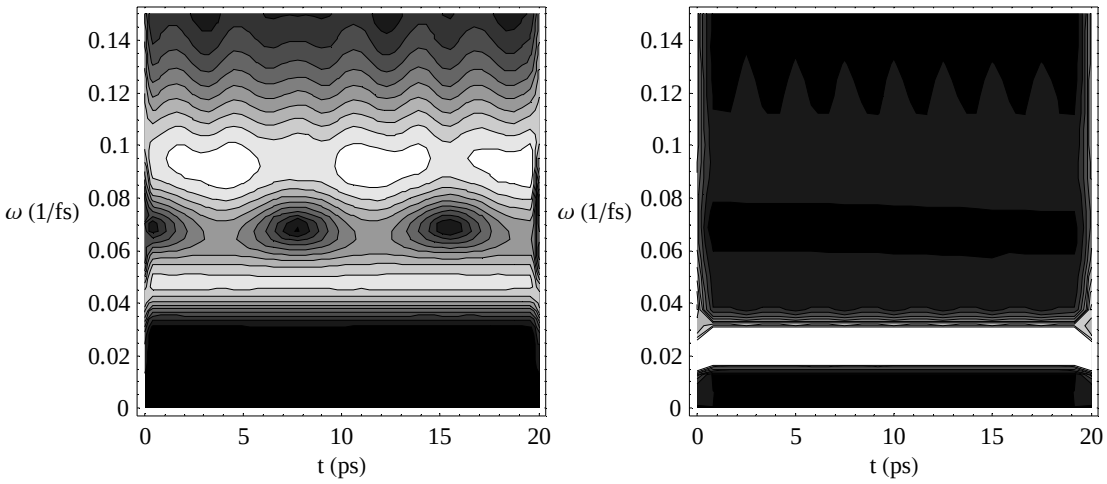

Figure 4-12: The wavelet transform contour plots are given for the center atom (left) and end atoms (right).

4.2.3 Hydrogen in a Silicon Lattice

The final sets of data analyzed with our wavelet technique are from a simulation of hydrogen atoms surrounded by a silicon lattice. The data – from D. West and S. Estreicher's work studying decay channels [46] – is in the form of x, y, and z coordinates of the hydrogen and silicon atoms taken at 0.3fs time steps over several hundred picoseconds. Physically, the simulation is a cubic cell approximately 10Å on

a side containing 62 atoms arranged in a geometry similar to diamond. Two silicon vacancies are present near the center of the cell and periodic boundary conditions are employed at the edges to extend the cell into a lattice. Two far more energetic hydrogen atoms fill these vacancies and are bonded to the surrounding silicons with dangling bonds. The hydrogen atom separation is greater than 3Å preventing hydrogen molecule formation.

The time series here are interesting because the energetic hydrogen atoms pass their energy to the (initially dull) surrounding lattice in order to bring the system into thermal equilibrium. However, the separation between the relatively high vibrational frequency of the hydrogen atom and the lower frequency silicon lattice continuum is large and so the hydrogen energy loss to the silicon occurs slowly. As demonstrated with the pendulums in Section 4.3.1, wavelet analysis can be used to study this energy transfer and trace how frequency and amplitude evolve.

Our analysis is divided into two sections. The first deals with the wavelet transform of one of the raw position series of one atom of hydrogen. This time series allows us to see how the system behaves near the initial source of the energy. Surprisingly, we are able to infer a lot about the entire system from just this data. The second section deals with a velocity autocorrelation time series that we constructed. This series allows us to gauge the behavior of the entire lattice at once. The smoothing washes out individual atom information, but therefore gives a better description of the bulk properties more analogous to what experimentalists investigate in the lab.

4.2.3.1 Hydrogen, x *Coordinate*

With 64 atoms and 3 coordinates, there are 192 series from the raw data alone. It may therefore seem a bit arbitrary to choose to look at only one of these (the *x* coordinate of one of the hydrogen atoms). As will be quickly seen though, the fact that all the expected dynamics fall out immediately and clearly is a strong argument for the sufficiency of one series, at least as a starting point. The other individual series are addressed briefly in Section 5.2 and a more general series is considered in the next section.

Before examining the wavelet transform, we again look at the Fourier transform (Figure 4-13). The plot shows an isolated strong peak near 60THz and a wide group of peaks in the low frequency range of 0-20THz. Experiments have shown that the density of states of crystalline silicon fills the frequency range of about 2-16THz [47], so it is reasonable to associate the peaks in this range to silicon. Also, we expect a single, higher frequency for the vibration of hydrogen, so we shall assume that the higher-valued peak is representative of that. This assumption is consistent with reported values for hydrogen in [48]. Thus, our wavelet transform should give similar results, but should also reveal information about how the amplitudes of these frequencies change with time.

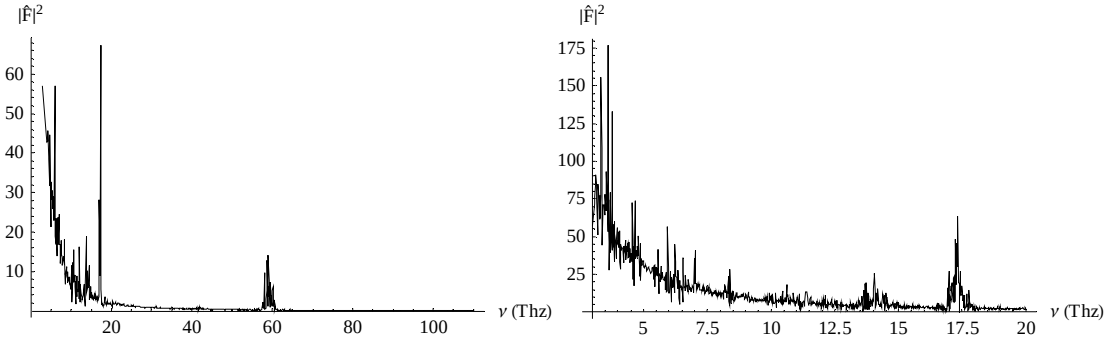

Figure 4-13: Fourier plots of the *x* coordinate series of one of the hydrogen atoms. The left plot is the entire spectrum of interest while the right plot shows the silicon density of states region.

Computing the wavelet transform on this series proved tricky. The enormous number of data points in the series (recall that it is several hundred picoseconds sampled at steps of 0.3fs) precluded us from examining the entire series at once; the largest time interval that could efficiently be examined without losing resolution for high frequencies was 4.8ps. This did not inhibit too greatly though. Certain traits (e.g. ridge extractions, time averages) could be extracted from each interval and compiled or the interval could be viewed independently to investigate short time scale behavior.

Over all intervals, the transforms gave results consistent with the Fourier analysis (Figure 4-14). A strong ridge is found at 60THz with a weaker peak at 120THz that is an anharmonic component (twice the primary hydrogen frequency value). The extracted amplitude of the ridge of the hydrogen frequency showed little significant variation over each interval (Figure 4-15), but piecing together the results over many intervals does show the expected slow decrease representing energy decay (Figure 4-16). A wide band of ridges and peaks in the low frequency range of about 0-20THz is also clearly seen. Over short periods, the band seems a jumbled mess, but

taking the time average over each interval gives a plot that approximates the silicon density of states (Figure 4-17).

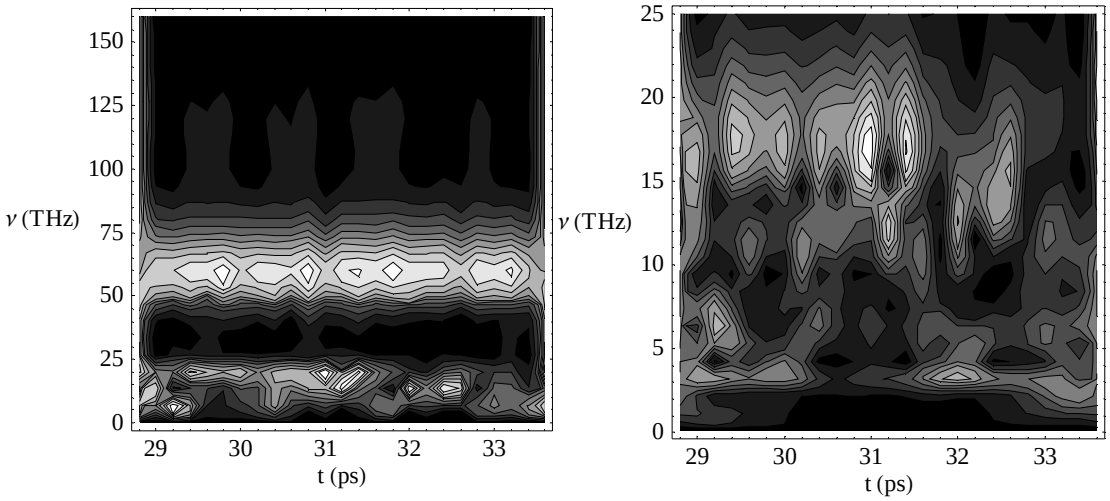

Figure 4-14: Wavelet plots of an interval of the hydrogen position data. On the left is the full spectrum. Note the primary hydrogen frequency around 60THz, the silicon density of states from ~0-25THz and the (hint of) anharmonic hydrogen frequency at 120THz. On the right is a blow-up of the density of states region.

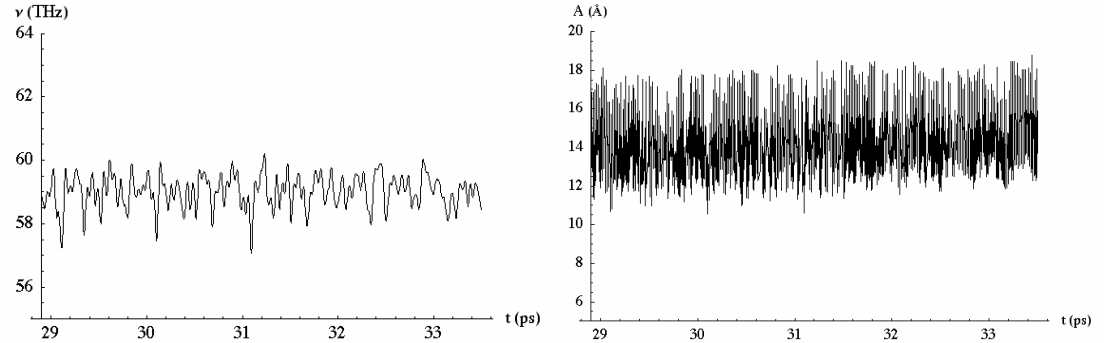

Figure 4-15: The extracted frequency and amplitude for the hydrogen ridge.

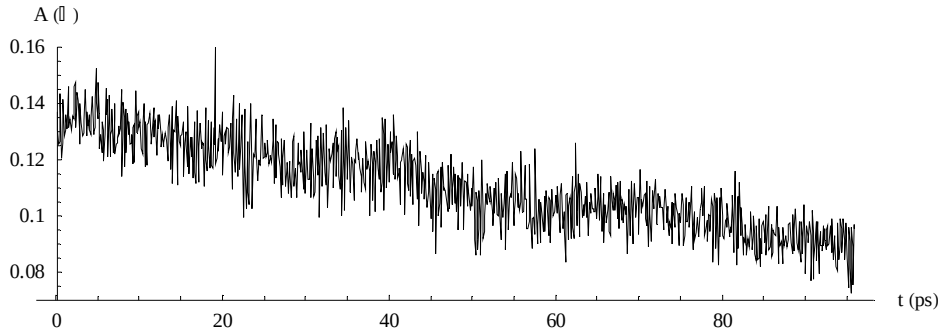

Figure 4-16: The slow decay of the hydrogen frequency's amplitude caused by its loss of energy to the surrounding lattice.

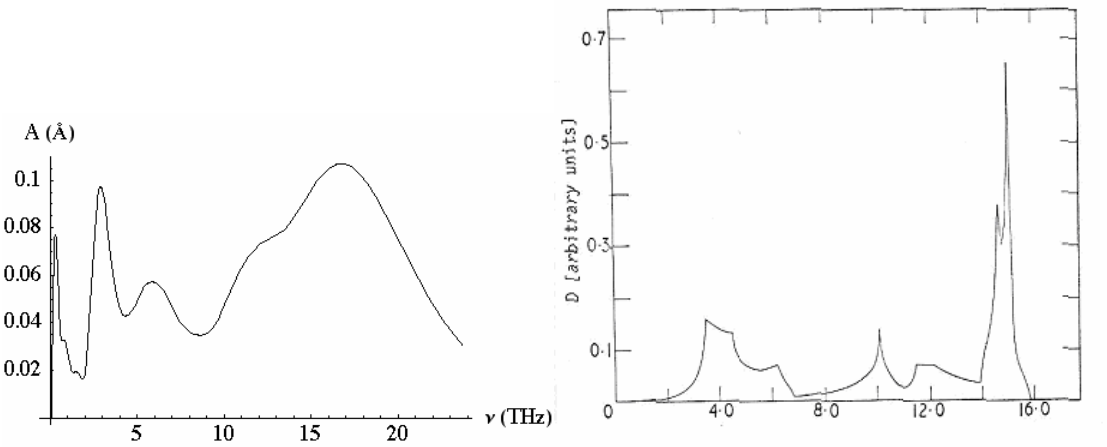

Figure 4-17: On the left, the density of states of silicon as recovered by averaging the wavelet transform over time for each frequency is shown. On the right is the experimentally determined density of states. (Source: [47].) Note the presence of important peaks near 4, 6, 12 and 16THz that appear in both.[25]

Recovering the silicon density of states over longer intervals shows that the results are consistent with physical interpretation, but this short term variation is interesting. Our best interpretation is that it represents quick energy transfer between the silicon and hydrogen modes as well as (probably) energy transfer within the silicon band. This inter-silicon transfer may be between the optical and acoustic parts of the

[25] The presence of low frequency components (below about 2THz) in the wavelet-derived density of states is to be expected due to the finite size of the simulation. These low frequencies only cancel out in the limit of many independent atoms.

range[26] or there may even be a continuum of exchange among all the frequencies in the range. Limitations in the wavelet transform prevent us from a definitive answer. Particularly the frequency resolution is not fine enough to give sharp peaks that can be differentiated from each other. The overlap of the wide peaks in the optical range with peaks in the acoustic range is particularly damaging.

It is in many ways remarkable that the wavelet spectrum of this single atom is so rich. Part of the reason is that the hydrogen atom we looked at was bonded to a silicon atom. Therefore, as the silicon atom vibrates with the rest of the lattice, some of that motion must appear in the hydrogen atom as well. Also, because hydrogen (atomic weight of ~1) is a much lighter atom than the silicon (atomic weight ~28), a small amplitude silicon oscillation is amplified tremendously when it is passed to the hydrogen. (Recall the harmonic oscillator energy formula, $E = \frac{1}{2} m\omega^2 A^2$.)

4.2.3.2 Velocity Autocorrelation

Next, we attempt to study the bulk behavior of the system by looking at the velocity autocorrelation series given by

$$g_i = \sum_{n=1}^{N} \vec{v}_n(t_i) \cdot \vec{v}_n(0)$$

where n is the atom number and N=64 is the total number of atoms. The series can be considered a characterization of the net displacement from initial conditions at each time step.

[26] Acoustic and optical vibrations are two different types of phonons in a solid. In our silicon lattice, the acoustic range is roughly that which falls below 7THz while the optical range is roughly 7-16THz.

As we did with the hydrogen atom, we first perform the Fourier transform (Figure 4-18). Again the hydrogen frequency and the silicon density of states are present. The anharmonic frequency at 120THz that appeared in the previous wavelet transform shows up too, as well as an additional anharmonic at 180THz (three times the primary hydrogen frequency).

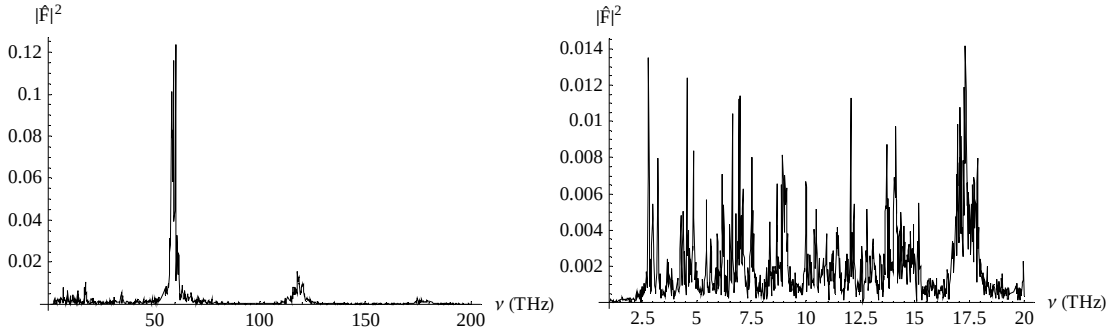

Figure 4-18: The Fourier transform of the velocity autocorrelation series. On the left is the full spectrum of interest. Notice the high peak for the hydrogen frequency as well as smaller peaks at its anharmonics of 120THz and 180THz. On the right is a blow-up of the behavior in the lattice vibration region.

Performing the wavelet transform gives plots similar to those seen for the single hydrogen, however with a slight difference (Figure 4-19 and Figure 4-20). In the hydrogen plots, the amplitudes of the hydrogen and silicon vibrations were comparable, but here the hydrogen amplitude is initially nearly an order of magnitude larger. This plot better represents the true energy dominance of the hydrogen vibrations that was distorted in the case above; the hydrogen atoms begin with far more energy and oscillate with larger amplitudes due to their smaller masses. Time averaging the intervals again recovers the density of states (Figure 4-21) and the long

time decay of the hydrogen amplitude (and therefore the energy) is seen as well (Figure 4-22).

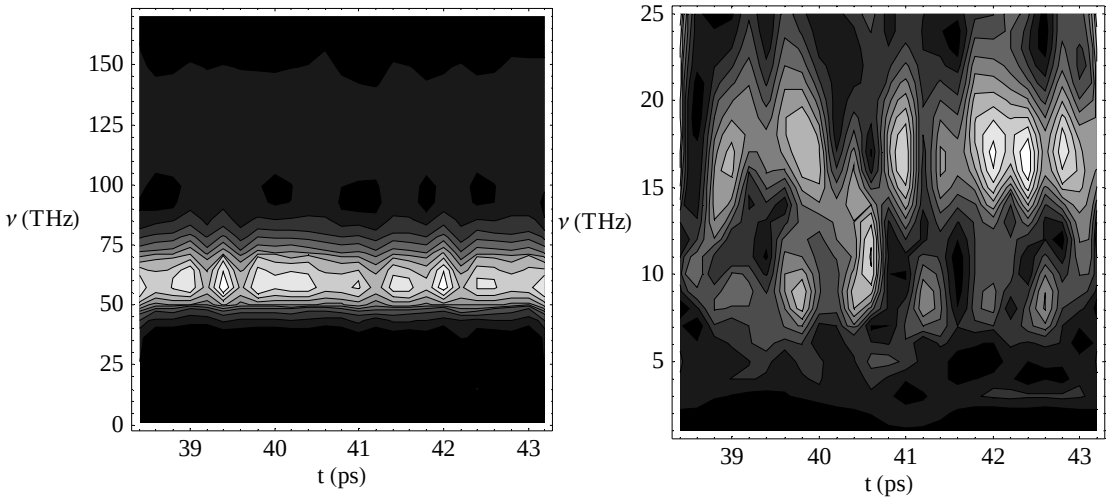

Figure 4-19: Wavelet plots showing the full spectrum (left) and the density of states region (right).

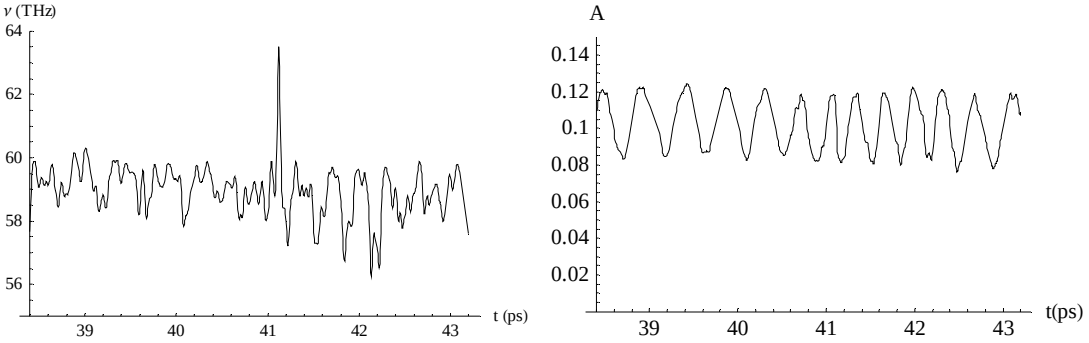

Figure 4-20: The extracted frequency (left) and amplitude (right) for the hydrogen ridge.[27]

[27] The apparent oscillation is an artifact of the transform related to wavelet choice. The wavelet parameter σ for this transform produced artificial oscillations similar to those seen in when using real-valued wavelets. (See Section 2.1.3.)

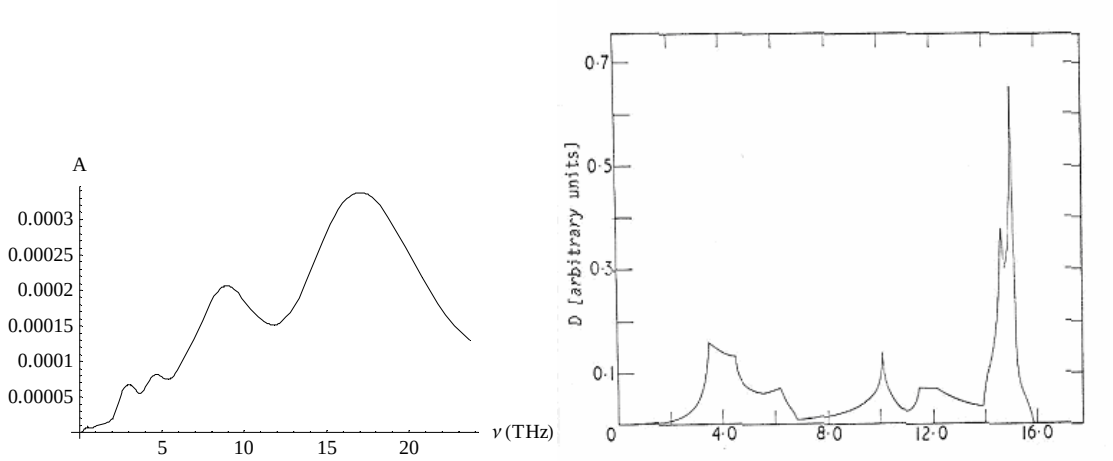

Figure 4-21: The recovered density of states, again compared to experimental values (Source: [47].)

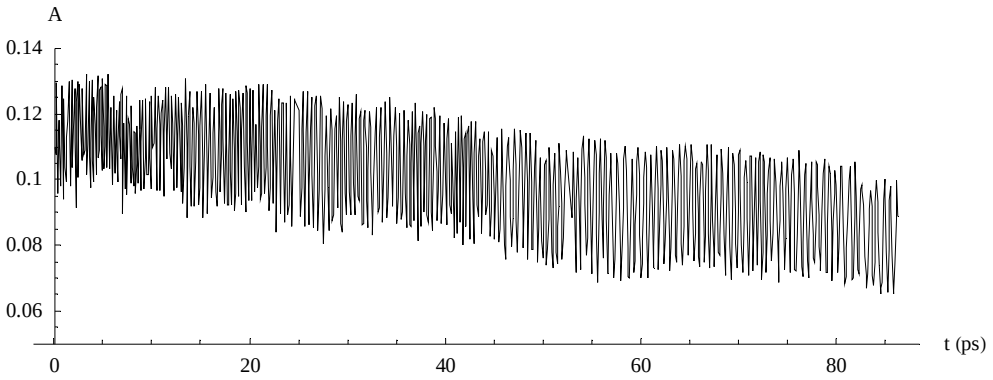

Figure 4-22: The decreasing amplitude of the hydrogen atom implying energy decay.

As with the single hydrogen, there is again substantial short-time scale energy transfer representing possible inter-silicon energy transfer or silicon-hydrogen transfer.

Chapter 5 Conclusions

5.1 The Wavelet Transform

This thesis has shown that the continuous wavelet transform is an effective tool for spectral estimation of non-stationary signals. Determining the frequency and amplitude of signal components as functions of time allows a wider range of possibilities than conventional (primarily Fourier-based) techniques. Many uses of the transform (such as the investigation of energy transfer we heavily pursued) are completely impossible without wavelet techniques. Non-stationary signals simply require time-frequency analyses such as the wavelet transform; stationary Fourier techniques will not do.

This thesis can also serve as a blueprint. The comprehensive review of wavelet techniques in Chapter 2 and the discussion of the specific implementation of those techniques with the Hilbert-Hermitian wavelet and the *Mathematica Time-Frequency Analysis* add-on in Chapter 3 can be used to jump-start a spectral estimation project. Wavelet transform implementation is simple and straightforward and other simple guides exist for the beginner.[28]

[28] Particularly good sources of information for beginners can be found in [7] and [20].

5.2 Further Study: Hydrogen and Silicon Lattice

Our study of the hydrogen and silicon lattice system was the primary application of the wavelet transform here. While we revealed useful information about the energy transfer problem that had not been found elsewhere, further study may be necessary to reap full knowledge from the data. Some of this further study certainly should involve the wavelet transform.

First, our analysis focused on only two time series: one coordinate of one hydrogen atom and the autocorrelation function. It might be helpful to look at other series. Position series of silicon atoms far from the center would certainly be different from the hydrogen, but by how much? We were initially surprised to see so much silicon information in our series. Perhaps, the inverse (a surprising amount of hydrogen information far away) is available as well. Also, velocity series or other autocorrelation series might reveal new information or frame it in a different way.

Next, we had hoped to determine the propagation speed of the energy from the hydrogen to the surrounding silicon lattice. Assuming normal wave propagation, $\omega = ck$, the speed of sound c in the system should be calculable and could be compared to any determined values. The most intuitive method is to look at some quantity related to energy, say velocity squared, and see how this quantity evolves over time for atoms increasingly farther from the center. Our simple attempts at this failed. Perhaps, however, it might be possible to use wavelet plots of the position or velocity series of atoms; one could identify an important event in the transforms of atoms near the hydrogen (e.g. some strong oscillations at a given frequency), and

search for the propagation of this event into the surrounding atoms. Not only might this yield propagation speed, but the study of how this event changes as it propagates could be interesting as well. The propagation speed, in fact, is probably quite anisotropic because of the lattice structure. For another completely different approach, the problem could be viewed from the point of thermal conductivity, possibly utilizing Kubo formulas [48], [49]. Here again, the signal information derived from wavelet plots might be useful.

Finally, another idea worth looking into would be a determination of expected energy transfer rates. It may be possible to rederive "Fermi's golden rule," normally applied to quantum transitions, to the phonon case here. For quantum mechanics, the transition rate is given by

$$\Gamma_{i\to f} = \frac{2\pi}{\hbar}\left|\langle f\left|H'\right|i\rangle\right|^2 \rho$$

where $\left|i\right\rangle$ is the initial state, $\left|f\right\rangle$ is the continuum of final states, ρ is the final density of states and $\left|\langle f\left|H'\right|i\rangle\right|^2$ is the perturbation matrix element [50]. In the rederivation, the perturbation of the Hamiltonian would be replaced by a perturbation of the dynamical matrix, the density of states would be the known (or perhaps wavelet-derived) density of states for silicon, and the initial state would of course be the hydrogen high frequency mode. Calculated energy transfer rates could be compared to wavelet transform results to further quantify the wavelet's results and to provide a check on the plausibility of the results. Though this problem differs from the one

above, thermal conductivity theory and especially Kubo formulas may again be useful [51].

5.3 Further Study: Spectral Estimation with Wavelets

There are many possibilities for future exploration with wavelets; any series that exhibits non-stationary behavior is candidate. There are a few topics we encountered though, that seem particularly promising that would benefit greatly from a wavelet analysis.

In astronomy, blazars and gamma ray bursts are both emerging as sources of non-stationary light curves. Quasi-periodicities in optical and radio emissions of blazar AO 0235+16, for example, have changing periods spanning a wide range from 5-6 years to 11.2-11.5 years as determined by Fourier techniques [52]. Certain astronomical models necessitate quasi-periodicity like this, so further and more accurate study using techniques such as wavelet analysis is needed to support or discredit these various models. The very recent application of wavelets to the study of blazar PKS B0048-097 by [53] had just this in mind and they are using their results to justify new intense observational campaigns to collect more data for study. Some gamma ray burst models also call for quasi-periodicity (on time scales of seconds or minutes unlike years for blazars) that could be detected by wavelet analysis. Fourier attempts have been made [54], but wavelets are beginning to appear on the scene as well [55], [56].

Along this vein, we had access to data from M. Böttcher of Ohio University from the blazar 3C 66A multiwavelength campaign he led in 2003-2004 under the auspices of the Whole Earth Blazar Telescope (WEBT) [57]. This optical light curve time series showed some quasi-periodicity from initial investigations with Fourier techniques and a wavelet analysis may have shed further light on the subject. However, the observations were made over the span of several months from different locations around the globe, so the time points were not evenly spaced. Our *Mathematica* wavelet package could not easily deal with such highly non-uniform sampling and no meaningful results could be garnered. A custom program or perhaps other available software would be able to deal with this and a proper analysis could be achieved. The results, we feel, might be highly revealing.

Another astronomical system that has recently emerged ripe for wavelet techniques is the structure of the rings of Saturn. Work by J. A. Burns *et al.* has taken images of the rings from the recent Cassini probe mission and produced space series from them [58]. Wavelet analyses of these series reveal density waves within the rings that are caused by the many moons and satellites of the planet [59]. Their series are particularly noisy and the wavelet transform has allowed them to extract information simply unavailable from the raw images. This technique could be extended to other astronomical systems similar to the rings where density waves might be present.

References

[1] N. Delprat, B. Escudié, P. Guillemain, R. Kronland-Martinet, P. Tchamitchian, and R. Torrésani, “Asymptotic wavelet and Gabor analysis: Extraction of instantaneous frequencies,” *IEEE Transactions on Information Theory*, vol. 38, no. 2, pp. 644-664, Mar. 1992.

[2] A. Schuster, "On the investigation of hidden periodicities with application to a supposed 26 day period of meteorological phenomena," T*errestrial Magnetism*, vol. 3, pp. 13-41, 1898.

[3] G. L. Bretthorst, *Bayesian Spectrum Analysis and Parameter Estimation*. Heidelberg, Germany: Springer-Verlag, 1988.

[4] E. T. Jaynes, *Probability Theory.* Cambridge, UK: Cambridge University Press, 2003.

[5] D. Gabor, “Theory of communication,” *Journal of the Institute of Electrical Engineers*, vol. 903, p. 429, 1946.

[6] W. C. Lang and K. Forinash, “Time-frequency analysis with the continuous wavelet transform,” *American Journal of Physics*, vol. 66, no. 9, pp. 794-797, Sept. 1998.

[7] P. S. Addison, *The Illustrated Wavelet Transform Handbook.* Bristol, UK: Institute of Physics Publishing, 2002.

[8] B. B. Hubbard, *The World According to Wavelets.* Natick, Massachusetts: A K Peters, 1998.

[9] A. Grossmann and J. Morlet, "Decomposition of Hardy functions into square integrable wavelets of constant shape," *SIAM Journal on Mathematical Analysis,* vol. 15, p. 723, 1984.

[10] P. Goupillaud, A. Grossman, and J. Morlet, "Cycle-octave and related transforms in seismic signal analysis," *Geoexploration*, vol. 23, pp. 85-102, 1984.

[11] I. Daubechies, "Orthonormal bases of compactly supported wavelets," *Communication on Pure and Applied Mathematics*, vol. 41, p. 909, 1988.

[12] I. Daubechies, "The wavelet transform, time-frequency localization and signal analysis," *IEEE Transactions on Information Theory*, vol. 36, pp. 961-1005, 1990.

[13] I. Daubechies, *Ten Lectures on Wavelets*. Philadelphia: SIAM, 1992.

[14] J. D. Harrop, *Structural Properties of Amorphous Materials.* PhD Thesis, Cambridge University, UK, 2004.

[15] M. Unser and T. Blu, "Mathematical properties of the JPEG2000 wavelet filters," *IEEE Transactions on Image Processing*, vol. 12, no. 9, pp. 1080-1090, 2003.

[16] M. Rabbani and R. Joshi, “An overview of the JPEG 2000 still image compression standard,” *Signal Processing: Image Communication*, vol. 17, no. 1, pp. 3-48, 2002.

[17] J. S. Walker, “Wavelet-based Image Compression” in *The Transform and Data Compression Handbook*, K. R. Rao and P. C. Yip, Eds. Boca Raton, Florida: CRC Press, 2001.

[18] R., Hayder, Y. Chen, K. Parthasarathy, and R. Cohen, “Scalable Internet video using MPEG-4,” *Signal Processing: Image Communication*, vol. 15, pp. 95-126, 1999.

[19] D. L. Jones and R. G. Baraniuk, “Efficient approximation of continuous wavelet transforms,” *Electronic Letters*, vol. 27, no. 9, pp. 748-750, Apr. 1991.

[20] C. Torrence and G. P. Compo, “A practical guide to wavelet analysis,” *Bulletin of the American Meteorological Society*, vol. 79, no. 1, pp. 61-78, Jan. 1998.

[21] A. Arneodo, E. Bacry, and J. F. Muzy, “The thermodynamics of fractals revisited with wavelets,” *Physica* A, vol. 213. pp. 232-275, 1995.

[22] S. Mallat and W. H. Hwang, “Singularity detection and processing with wavelets,” *IEEE Transactions on Information Theory*, vol. 38, pp. 617-643, 1992.

[23] A. Arneodo, E. Bacry, and J. F. Muzy, “Oscillating singularities in locally self-similar functions,” *Physical Review Letters*, vol. 74, pp. 4823-4826, 1995.

[24] H. H. Szu, C. C. Hsu, L. D. Sa, and W. Li, “Hermitian hat wavelet design for singularity detection in the Paraguay river-level data analyses,” in *SPIE*

Proceedings on Wavelet Applications IV, (Orlando, FL), pp. 96-115, April 1997.

[25] "Continuous Wavelet Transform," *Seasolve,* [Online document], [cited 2007 May 15], Available HTTP: http://www.seasolve.com/products/autosignal/resources/htmlHelp/cont0040.html

[26] R. A. Carmona, W.L. Hwang, and B. Torrésani, "Characterization of signals by the ridges of their wavelet transforms," *IEEE Transactions on Signal Processing*, vol. 45, no. 10, pp. 2586-2590, Oct. 1997.

[27] R. A. Carmona, W. L. Hwang, and B. Torrésani, "Multiridge detection and time-frequency reconstruction," *IEEE Transactions on Signal Processing*, vol. 47, no. 2, pp. 480-492, Feb. 1999.

[28] R. Carmona, W. L. Hwang, and B. Torrésani, *Practical time-frequency analysis: Gabor and wavelet transforms with an implementation in S.* San Diego: Academic Press, 1998.

[29] Flying Frog Consultancy, *Time Frequency Analysis: Mathematica Add-on Package.* [Download], UK: Flying Frog Consultancy, 2005, Available HTTP: http://www.ffconsultancy.com/products/cwt/

[30] "Continuous wavelets and time-frequency analysis," *Flying Frog Consultancy,* [Online document], [cited 2006 Jan 1], Available HTTP: http://www.ffconsultancy.com/products/cwt/

[31] De Nyago Tafen, M. Mitkova, and D. A. Drabold, “Silver transport in Ge_xSe_{1-x}:Ag materials: *Ab initio* simulation of a solid electrolyte,” *Physical Review B,* vol 72, art. no. 054206, 2005.

[32] J. K. Christie, S. N. Taraskin, and S. R. Elliott, “Structural characteristics of positionally-disordered lattices: relation to the first sharp diffraction peak in glasses,” *Physical Review B*, vol. 70, art. no. 134207, 2004.

[33] M. Fligge, S. K. Solanki, and J. Beer, “Determination of solar cycle length variations using the continuous wavelet transform,” *Astronomy and Astrophysics*, vol. 346, pp. 313-321, 1999.

[34] S. L. Marple, *Digital Spectral Analysis with Applications*. New Jersey: Prentice-Hall, 1987.

[35] M. Waldmeier, *The Sunspot Activity in the Years 1610-1960.* Zurich: Schulthes, 1961.

[36] S. H. Schwabe, “Solar observations during 1843,” *Astronomische Nachrichten*, vol. 20, no. 495, pp. 234–235, 1843.

[37] A. Schuster, "On the periodicities of sunspots", *Philosophical Transactions of the Royal Society of London, Series A*, vol. 206, pp. 69-100, 1906.

[38] F. E. Olvera, Jr., “A spectral analysis of the sunspot time series using the periodogram,” [Online document], [cited 2007 May 24], Available HTTP: http://web.cecs.pdx.edu/~ssp/Reports/2005/Olvera.pdf

[39] S. Bhattacharyya and R. Naraimha, “Possible association between Indian monsoon rainfall and solar activity,” *Geophysical Research Letters*, vol. 32, art. no. L05813, 2005.

[40] R. E. Benestad, *Solar Activity and Earth's Climate*. Chichester, UK: Springer Praxis Books, 2002.

[41] G.-H. Lim, A.-S Suh, and Y. Suh, “Red Shift Phenomena Revealed in the Zonal Winds Oscillations Probably Induced by the Sunspot Cycle,” presented at 15th Symposium on Global Change and Climate Variations, American Meteorological Society, 2004.

[42] C. Torrence and G. Compo, *Wavelet Analysis Software*, HTTP: http://atoc.colorado.edu/research/wavelets/software.html

[43] “Joseph Fourier,” *Encyclopedia Britannica Online*. [cited 2007 May 30], Available HTTP: http://britannica.com/eb/article9035044

[44] D. A. Drabold, Personal communication, 2007 May 29.

[45] D. A. Drabold, R. P. Wang, S. Klemm, O. F. Sankey, and J. D. Dow, “Efficient ab initio molecular dynamics simulations of carbon,” *Physical Review B*, vol. 43, no. 6, 5132-5134, Feb. 1991.

[46] D. West and S. K. Estreicher, “First-principles calculations of vibrational lifetimes and decay channels: Hydrogen-related modes in Si,” *Physical Review Letters*, vol. 96, art. no. 115504, Mar. 2006.

[47] H. Bilz and W. Kress, *Phonon Dispersion Relations in Insulators.* Berlin: Springer-Verlag, 1979.

[48] P. B. Allen and J. L. Feldman, “Thermal conductivity of disorder harmonic solids,” *Physical Review B*, vol. 48, no. 17, pp. 12581-12588, 1993.

[49] J. L. Feldman, M. D. Kluge, P. B. Allen, and Frederick Wooten, “Thermal conductivity and localization in glasses: Numerical study of a model of amorphous silicon,” *Physical Review B*, vol. 48, no. 17, pp. 12589-12602, 1993.

[50] E. Fermi, *Nuclear Physics.* Chicago: University of Chicago Press, 1950.

[51] P. B. Allen and J. L. Feldman, “Thermal conductivity of glasses: Theory and application to amorphous Si,” *Physical Review Letters*, vol. 62, no. 6, 1989.

[52] C. M. Raiteri *et al.*, “Optical and radio variability of the BL Lacertae object AO 0235+16: A possible 5-6 year periodicity,” *Astronomy and Astrophysics,* vol. 377, pp. 396-412, 2001.

[53] M. Kadler, P. A. Hughes, E. Ros, M. F. Aller, and H. D. Aller, “A quasi-periodic modulation of the radio light curve of the blazar PKS B0048-097,” *Astronomy and Astrophysics*, vol. 456, pp. L1-L4, 2006.

[54] A. M. Beloborodov, B. E. Stern, and R. Svenson, “Power density spectra of gamma-ray bursts,” *The Astrophysical Journal*, vol. 535, pp. 158-166, May 2000.

[55] K. C. Walker, B. E. Schaefer, and E. E. Fenimore, “Gamma-ray bursts have millisecond variability,” *The Astrophysical Journal*, vol. 537, pp. 264-269, 2000.

[56] F. Quilligan, K. J. Hurley, B. McBreen, L. Hanlon, and P. Duggan, "Characteristic properties of peaks in GRBs," *Astronomy and Astrophysics Supplement Series,* vol. 138, pp. 419-420, 1999.

[57] M. Böttcher *et al*., "Coordinated multiwavelength observation of 3C 66A during the WEBT campaign of 2003-2004," *The Astrophysical Journal*, vol. 631, pp. 169-186, 2005.

[58] J. A. Burns, M. S. Tiscareno, C. C. Porco, H. Dones, C. D. Murray, and Cassini Imaging, "Weak waves and wakes in Saturn's rings: Observations by Cassini ISS," *AAS/Division for Planetary Sciences Meeting Abstracts*, vol. 36, art. no. 19.12, 2004.

[59] M. S. Tiscareno, J. A. Burns, P. D. Nicholson, M. M. Hedman, and C. C. Porco, "Cassini imaging of Saturn's rings II: A wavelet technique for analysis of density waves and other radial structure in the rings," preprint arXiv:astro-ph/0610242v3, 17 Jan 2007; *to appear in Icarus*.

Author's Note

I'd like to close with some artwork that I collected as I wrote this thesis. I don't believe there is another collection of wavelet inspired art anywhere in the world. I also don't believe that that this collection will start any trends to change that. Oh well. Enjoy!

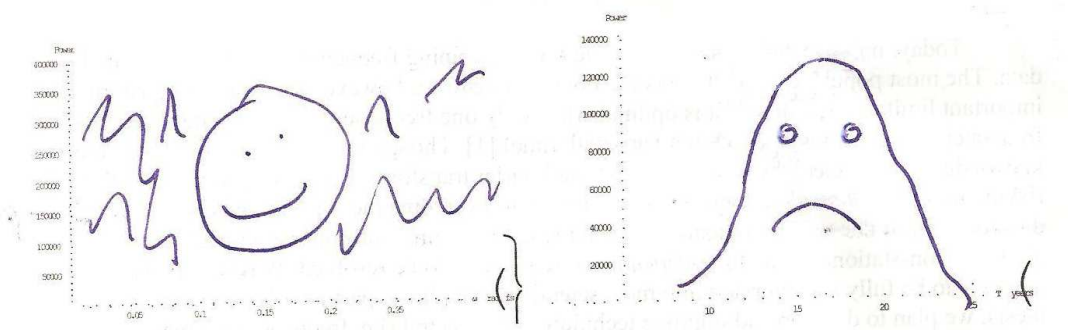

Figure 1: Fourier Periodograms
Each graph is a plot of the power spectrum (periodogram) for a given function. The graph on the left has very sharp peaks corresponding with very well defined, discrete frequencies. The graph on the right shows broad peaks representing a continuum of frequencies.

D. A. Drabold, October 3, 2006

-When my plots wouldn't print, Dr. Drabold didn't despair. He drew his own.

D. A. Drabold, April 24, 2007

-An illustration of the biologist's time series: number of salmon in a river over a given time period.

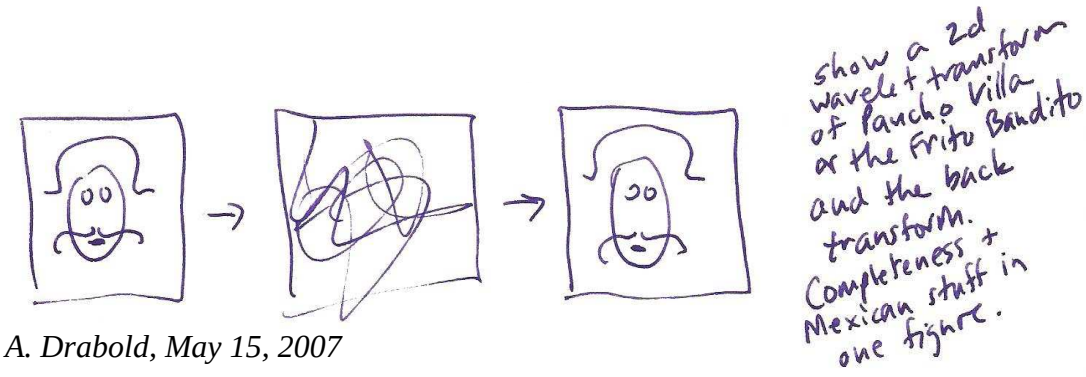

D. A. Drabold, May 15, 2007

-Rather than discuss the Mexican hat wavelet and the discrete wavelet transform's use in image compression separately, Dr. Drabold suggested that I combine the two.

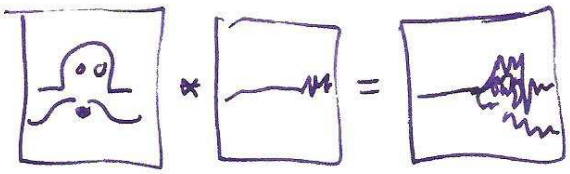

Figure 2-X: Wavelet Interpretation Plot

D. A. Drabold, May 15, 2007

-He also thought Pancho Villa might help me explain how the transform works. (See Figure 2-3.) I'm not sure that's the correct result for "Pancho" times "wavelet."

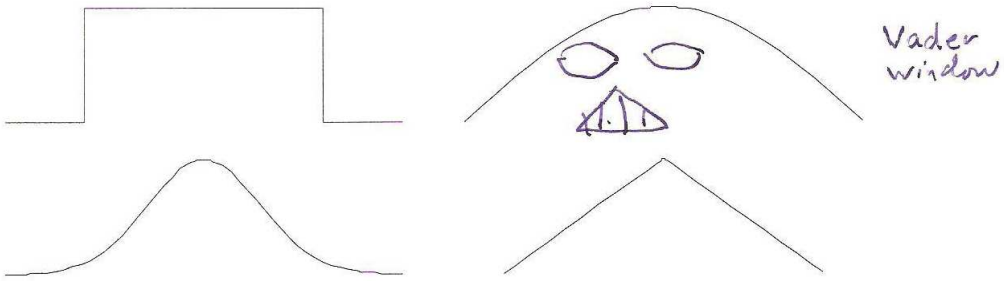

Figure 1-4: Examples of common window functions.

D. A. Drabold, May 25, 2007

-Since this a thesis about wavelets, I think it's appropriate to think of windows as members of the Dark Side.

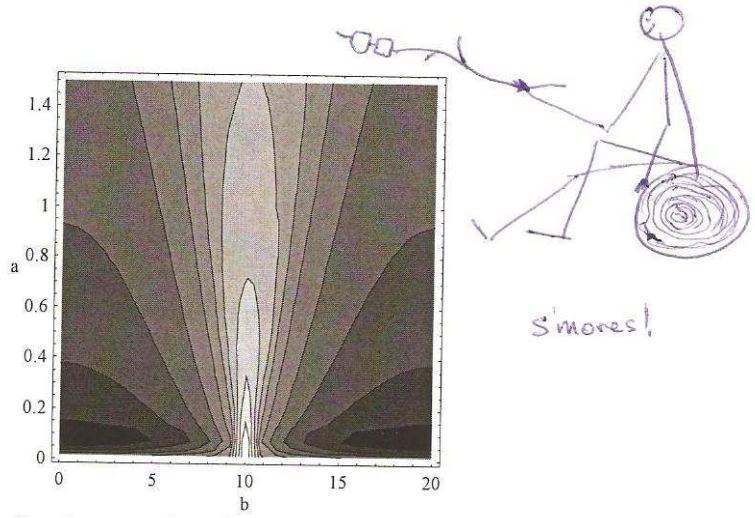

C. J. McCrone, May 31, 2007

-Relaxing after a long day of thesis writing!